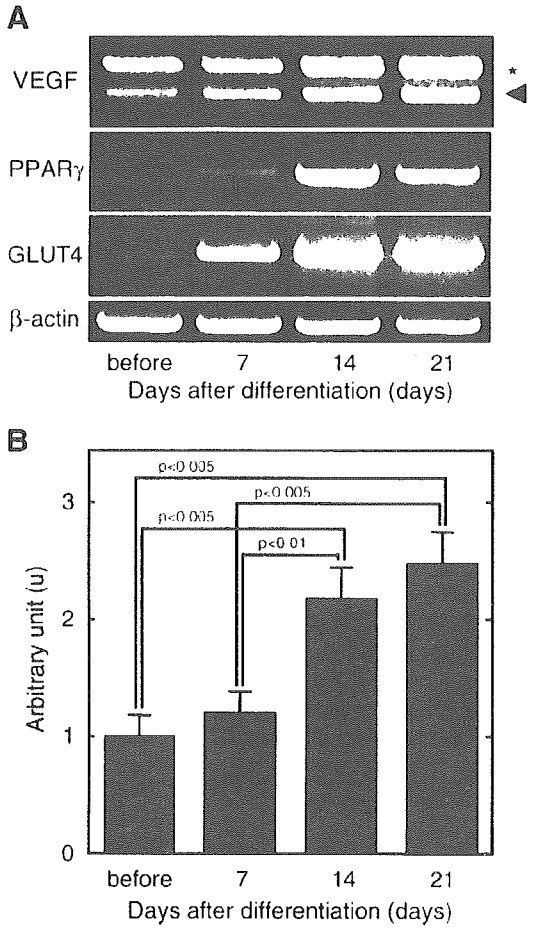

Fig. 7. Time course changes of VEGF, peroxisome proliferator-activated receptor-γ (PPARγ), and GLUT4 expressions in 3T3-L1 cells during adipocyte differentiation. *A*: gene expression profiles in 3T3-L1 cells during adipocyte differentiation. Images show RT-PCR products of VEGF, PPARγ, and GLUT4 amplified from total RNA in 3T3-L1 cells at 0, 7, 14, and 21 days after differentiation. *B*: relative amounts of VEGF expressions in 3T3-L1 cells during adipocyte differentiation. The PCR products of VEGF were densitometrically analyzed, and the relative amounts in predifferentiated 3T3-L1 cells were set to 1.0. Results are represented as means + SD. Arrowhead, $VEGF_{164}$; *, $VEGF_{188}$.

mice was significantly related to their body weight, the same as our previous results in human subjects (15). These results suggest that plasma VEGF may be determined by body fat deposition in mice.

In our previous report (15), plasma VEGF concentrations were revealed to be dependent on visceral fat accumulation. Therefore, to clarify the VEGF expressions with regard to whether subcutaneous or visceral adipose tissue affects plasma VEGF concentration in *db/db* mice, we examined mRNA expressions and protein contents of VEGF in visceral and subcutaneous adipose tissues during growth. The mRNA ex-

Table 1. *VEGF concentrations of conditioned media cultured with pre- and postdifferentiated 3T3-L1 cells*

	Days			
Differentiation periods	0	7	14	21
VEGF concentration, ng/ml	0.6±0.1	0.9±0.2	2.4±0.5	2.6±0.2
Total protein concentration, mg/ml	0.4±0.1	0.4±0.1	0.4±0.2	0.4±0.2

Values are means ± SD. VEGF, vascular endothelial growth factor.

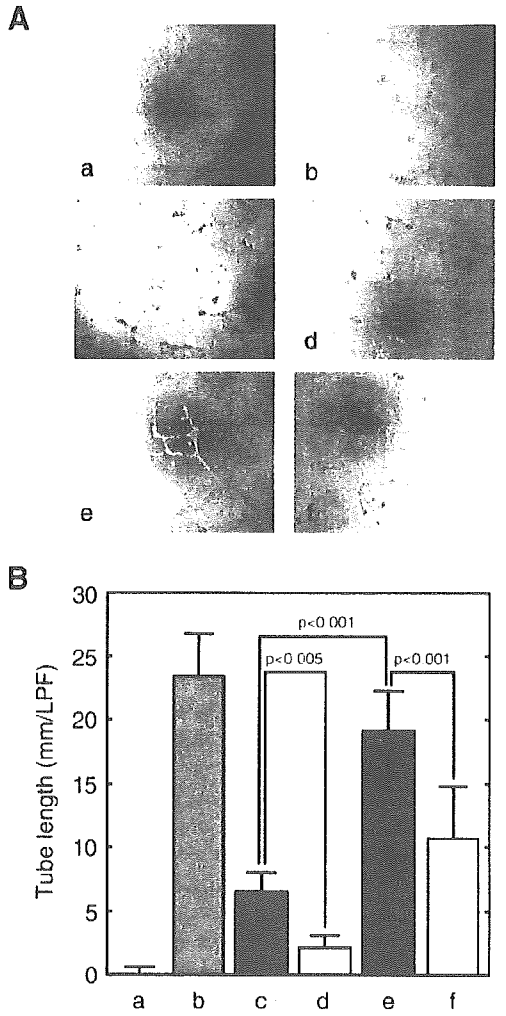

Fig. 8. Effect of conditioned media cultured with pre- and postdifferentiated 3T3-L1 cells on tube formation activity in human umbilical vein endothelial cells (HUVECs). *A*: light microscopic findings of tube formation of HUVECs in various conditions. Formation of capillary tube-like structures by HUVECs was assessed in a Matrigel-based assay as previously described (8). HUVECs were seeded on Growth Factor Reduced BD Matrigel matrix with conditioned medium derived from pre- or postdifferentiated 3T3-L1 cells in the presence or absence of anti-mouse VEGF-neutralizing antibody or recombinant VEGF protein. After 13 h of stimulation, phase-contrast microscopic low-power fields (×100) were photographed. *a*: medium alone; *b*: stimulated with recombinant VEGF (5 ng/ml); *c* and *d*: with conditioned medium from predifferentiated 3T3-L1 cells; *e* and *f*: with conditioned medium from postdifferentiated 3T3-L1 cells; *c* and *e*: in the absence of anti-VEGF antibody; *d* and *f*: in the presence of anti-VEGF antibody. *B*: tube length of HUVECs stimulated with conditioned medium prepared from pre- or postdifferentiated 3T3-L1 cells. The total length of capillary tubes formed by HUVECs in 3 different photographs per well were measured using a scale ruler. *Bar a*, medium alone; *bar b*, recombinant VEGF (5 ng/ml); *bar c*, conditioned medium from predifferentiated 3T3-L1 cells alone; *bar d*, conditioned medium from predifferentiated 3T3-L1 cells with anti-VEGF antibody; *bar e*, conditioned medium from postdifferentiated 3T3-L1 cells alone; *bar f*, conditioned medium from postdifferentiated 3T3-L1 cells with anti-VEGF antibody.

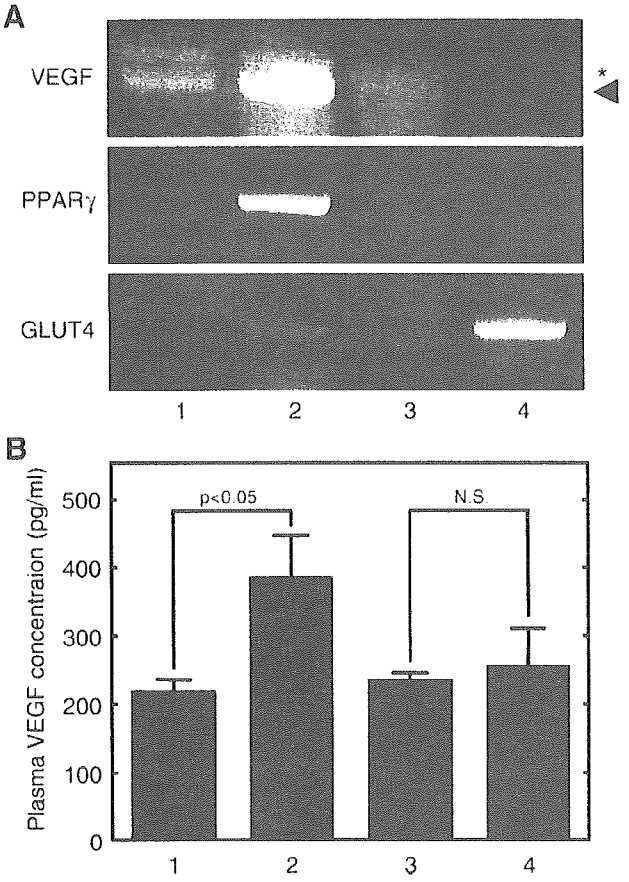

Fig. 9. Comparison of VEGF, PPARγ, and GLUT4 expressions among mice implanted with 3T3-L1 cells into mesenteric or subcutaneous fat area and controls. *A*: gene expression profiles in 3T3-L1 cells implanted into adipose tissues of nude mice. Images show RT-PCR products of VEGF, PPARγ, and GLUT4 amplified from total RNA in adipose tissues. *Lane 1*, mesenteric adipose tissues injected with PBS alone; *lane 2*, mesenteric adipose tissues injected with 3T3-L1 cells; *lane 3*, subcutaneous adipose tissues injected with PBS alone; *lane 4*, subcutaneous adipose tissues injected with 3T3-L1 cells. Arrowhead, $VEGF_{164}$; *, $VEGF_{188}$. *B*: plasma VEGF concentrations in mice implanted with 3T3-L1 cells. Plasma VEGF concentrations were measured at 4 wk after implantation with 3T3-L1 cells. *Lane 1*, mice injected with PBS alone into mesenteric area; *lane 2*, mice injected with 3T3-L1 cells into mesenteric area; *lane 3*, mice injected with PBS alone into subcutaneous area; *lane 4*, mice injected with 3T3-L1 cells into subcutaneous area.

pression levels of VEGF in visceral fat were more enhanced than in subcutaneous fat. Furthermore, the protein contents were enhanced in visceral fat but not in subcutaneous fat. These results suggest that plasma VEGF concentrations are revealed to be dependent on visceral fat accumulation even in mice.

The expression levels of TNF-α and PAI-1 in adipocytes are reported to be directly related to the degree of differentiation from preadipocytes and to be dependent on their anatomic location (12, 14, 20, 21). Therefore, we demonstrated the degree of fat accumulation in adipocytes and the correlation between VEGF mRNA expressions and adiposity in subcutaneous and mesenteric adipose tissues. Whole tissue weights of mesenteric and subcutaneous fat were increased gradually during growth. However, total cell counts were significantly decreased during growth in mesenteric fat but not in subcutaneous fat. A significant correlation between VEGF mRNA expressions and weight and adiposity in mesenteric adipose tissue was observed, but not in subcutaneous adipose tissue. These results suggest that the increase of weight in mesenteric adipose tissue is dependent on fat accumulation in adipocytes but not in subcutaneous adipose tissue. Moreover, VEGF expression is dependent on the levels of fat deposition in adipocytes. Then, we isolated the adipocyte fraction from mesenteric fat and examined VEGF mRNA expression in adipocytes. VEGF expression levels in the adipocyte fraction were also increased during growth.

Next, we examined the relation between VEGF expression and degree of differentiation using 3T3-L1 cells, an established adipocyte cell line. VEGF mRNA was expressed even in the preadipocyte condition, and its expression was enhanced after adipocyte conversion. Especially, the expression levels of VEGF mRNA were significantly increased 14 days after differentiation. Furthermore, the levels of VEGF protein secretion were almost the same level as gene expression. These results suggest that VEGF production may be dependent on the lipid accumulation (maturation) as well as the time lapse after adipocyte conversion rather than adipocyte differentiation from preadipocytes in 3T3-L1 cells.

We next determined whether VEGF protein secreted from 3T3-L1 cells has some biological activities. To know the role of VEGF in physiological or pathological conditions, we examined the effect of conditioned medium derived from 3T3-L1 cells on in vitro tube formation activity in HUVECs. The conditioned media from pre- and postdifferentiated 3T3-L1 cells enhanced angiogenesis in vascular endothelial cells. These results suggest that VEGF protein secreted from adipocytes may play some roles in the pathological neovascularization observed in diabetic retinopathy or atherosclerosis.

In the third set of experiments, the effects of anatomic localization on fat accumulation and VEGF production in adipocytes were analyzed using a cell implantation technique. 3T3-L1 cells implanted into the mesenteric area of athymic mice expressed more VEGF mRNA than that implanted into the subcutaneous area. The expression of PPARγ was also higher in 3T3-L1 cells implanted into the mesenteric area than into the subcutaneous area, and plasma VEGF concentrations in the mice implanted with 3T3-L1 cells into the mesenteric area were higher than in the subcutaneous area. These results suggest that a certain mechanism may exist in the visceral fat area to make implanted 3T3-L1 cells for enhanced VEGF production.

In summary, these results from in vitro and in vivo experiments indicate that VEGF expression in adipocytes is possibly differentiation as well as time (age) dependent after adipocyte conversion and may be determined by the site of body distribution. Further experiments are required to clarify the mechanism of enhanced expression of VEGF in visceral fat.

GRANTS

These studies were supported by grants from the Japanese Ministry of Education, Science, Sports and Culture.

REFERENCES

1. **Afuwape AO, Kiriakidis S, and Paleolog EM.** The role of the angiogenic molecule VEGF in the pathogenesis of rheumatoid arthritis. *Histol Histopathol* 17: 961–972, 2002.
2. **Aiello LP, Avery RL, Arrigg PG, Keyt BA, Jampel HD, Shah ST, Pasquale LR, Thieme H, Iwamoto MA, Park JE, Nguyen HV, Aiello LM, Ferrara N, and King GL.** Vascular endothelial growth factor in ocular fluid of patients with diabetic retinopathy and other retinal disorders. *N Engl J Med* 331: 1480–1487, 1994.
3. **Chiarelli F, Spagnolit A, Basciani F, Tumini S, Mezzetti A, Cipollone F, Cuccurullo F, Morgese G, and Verrotti A.** Vascular endothelial growth factor (VEGF) in children, adolescents and young adults with Type 1 diabetes mellitus: relation to glycaemic control and microvascular complications. *Diabet Med* 17: 650–656, 2000.
4. **Claffey KP, Wilkison WO, and Spiegelman BM.** Vascular endothelial growth factor. Regulation by cell differentiation and activated second messenger pathways. *J Biol Chem* 267: 16317–16322, 1992.
5. **Dvorak HF, Brown LF, Detmar M, and Dvorak AM.** Vascular permeability factor/vascular endothelial growth factor, microvascular hyperpermeability, and angiogenesis. *Am J Pathol* 146: 1029–1039, 1995.
6. **Ferrara N.** Role of vascular endothelial growth factor in physiologic and pathologic angiogenesis: therapeutic implications. *Semin Oncol* 6: 10–14, 2002.
7. **Hotamisligil GS, Arner P, Caro JF, Atkinson RL, and Spiegelman BM.** Increased adipose tissue expression of tumor necrosis factor-α in human obesity and insulin resistance. *J Clin Invest* 95: 2409–2415, 1995.
8. **Kubota Y, Kleinman HK, Martin GR, and Lawley TJ.** Role of laminin and basement membrane in the morphological differentiation of human endothelial cells into capillary-like structures. *J Cell Biol* 107: 1589–1598, 1988.
9. **Leung DW, Cachianes G, Kuang WJ, Goeddel DV, and Ferrara N.** Vascular endothelial growth factor is a secreted angiogenic mitogen. *Science* 246: 1306–1309, 1989.
10. **MacDougald OA, Hwang CS, Fan H, and Lane MD.** Regulated expression of the obese gene product (leptin) in white adipose tissue and 3T3-L1 adipocytes. *Proc Natl Acad Sci USA* 92: 9034–9037, 1995.
11. **Madrup S, Loftus TM, MacDougald OA, Kuhajda FP, and Lane MD.** Obese gene expression at in vivo levels by fat pads derived from s.c. implanted 3T3-F442A preadipocytes. *Proc Natl Acad Sci USA* 94: 4300–4305, 1997.
12. **Maeda K, Okubo K, Shimomura I, Mizuno K, Matsuzawa Y, and Matsubara K.** Analysis of an expression profile of genes in the human adipose tissue. *Gene* 190: 227–235, 1997.
13. **Matsumoto F, Bujo H, Kuramochi D, Saito K, Shibasaki M, Takahashi K, Yoshimoto S, Ichinose M, and Saito Y.** Effects of nutrition on the cell survival and gene expression of transplanted fat tissues in mice. *Biochem Biophys Res Commun* 295: 630–635, 2002.
14. **Mertens I, Van der Planken M, Corthouts B, Wauters M, Peiffer F, De Leeuw I, and Van Gaal L.** Visceral fat is a determinant of PAI-1 activity in diabetic and non-diabetic overweight and obese women. *Horm Metab Res* 33: 602–607, 2001.
15. **Miyazawa-Hoshimoto S, Takahashi K, Bujo H, Hashimoto N, and Saito Y.** Elevated serum vascular endothelial growth factor is associated with visceral fat accumulation in human obese subjects. *Diabetologia* 46: 1483–1488, 2003.
16. **Paleolog EM.** Angiogenesis in rheumatoid arthritis. *Arthritis Res* 4: S81–S90, 2002.
17. **Ross JS, Stagliano NE, Donovan MJ, Breitbart RE, and Ginsburg GS.** Atherosclerosis: a cancer of the blood vessels? *Am J Clin Pathol* 116: S97–S107, 2001.
18. **Senger DR, Van de Water L, Brown LF, Nagy JA, Yeo KT, Yeo TK, Berse B, Jackman RW, Dvorak AM, and Dvorak HF.** Vascular permeability factor (VPF, VEGF) in tumor biology. *Cancer Metastasis Rev* 12: 303–324, 1993.
19. **Shibasaki M, Takahashi K, Itou T, Miyazawa S, Ito M, Kobayashi J, Bujo H, and Saito Y.** Alterations of insulin sensitivity by the implantation of 3T3-L1 cells in nude mice. A role for TNF-alpha? *Diabetologia* 45: 518–526, 2002.
20. **Shimomura I, Funahashi T, Takahashi M, Maeda K, Kotani K, Nakamura T, Yamashita S, Miura M, Fukuda Y, Takemura K, Tokunaga K, and Matsuzawa Y.** Enhanced expression of PAI-1 in visceral fat: possible contributor to vascular disease in obesity. *Nat Med* 2: 800–803, 1996.
21. **Tsigos C, Kyrou I, Chala E, Tsapogas P, Stavridis JC, Raptis SA, and Katsilambros N.** Circulating tumor necrosis factor alpha concentrations are higher in abdominal versus peripheral obesity. *Metabolism* 48: 1332–1335, 1999.
22. **Vozarova B, Weyer C, Hanson K, Tataranni PA, Bogardus C, and Pratley RE.** Circulating interleukin-6 in relation to adiposity, insulin action, and insulin secretion. *Obes Res* 9: 414–417, 2001.

ELSEVIER

Atherosclerosis 178 (2005) 1–7

ATHEROSCLEROSIS

www.elsevier.com/locate/atherosclerosis

A potent activator of PPARα and γ reduces the vascular cell recruitment and inhibits the intimal thickning in hypercholesterolemic rabbits

Naoto Seki[a], Hideaki Bujo[b,*], Meizi Jiang[b], Manabu Shibasaki[a], Kazuo Takahashi[a], Naotake Hashimoto[c], Yasushi Saito[a]

[a] *Department of Clinical Cell Biology (F5), Graduate School of Medicine, Chiba University, Chiba 260-8670, Japan*
[b] *Department of Genome Research and Clinical Application (M6), Graduate School of Medicine, Chiba University, 1-8-1 Inohana, Chuo-ku, Chiba 260-8670, Japan*
[c] *Division of Applied Translational Research, Graduate School of Medicine, Chiba University, Chiba 260-8670, Japan*

Received 15 February 2004; received in revised form 18 July 2004; accepted 10 August 2004
Available online 27 September 2004

Abstract

Peroxisome proliferator-activated receptors (PPARs) regulate the vascular cell functions as well as systemic lipid and glucose metabolism. Here, we studied the effect of TAK-559, a newly developed potent activator both for PPARα and γ, on the vascular cell recruitment. TNF-α - or interleukin-1β (IL-1β)-induced THP-1 cell attachment to cultured endothelial cells was significantly reduced in the presence of 10 μM TAK-559 ($P < 0.05$). The secretion of monocyte chemoattractant protein-1 (MCP-1) from endothelial cells is reduced by 36% in the presence of 10 μM TAK-559, accompanied with the decreased mRNA expression in the cells. The proliferation and migration of cultured smooth muscle cells (SMCs) were significantly decreased in the presence of TAK-559 ($P < 0.05$). TAK-559-treated hypercholesterolemic rabbits showed the significant reduction of intimal thickning after balloon catheterization by 51% compared with control ($P < 0.05$), although the plasma lipid and glucose level was not changed between them. The numbers of macrophage and SMCs were decreased to 34% and 49% in the hyperplastic intima of arteries from TAK-559-treated rabbits compared to those from control, respectively. These results suggest that the PPARα and γ activator inhibits the recruitment of macrophages and SMCs in intima, possibly leading to the reduction of intimal hyperplasia in hypercholesterolemia.

Keywords: Peroxisome proliferator-activated receptors; Vascular wall; Hypercholesterolemia; Intimal thickning

1. Introduction

Peroxisome proliferator-activated receptors (PPARs) are nuclear receptors, and play an important role in the regulation of vascular cell functions as well as of systemic lipid and glucose metabolism, possibly leading to the inhibition of progression of athrosclerosis [1]. One of PPARs, PPARγ, is inclusively expressed in the arterial wall, such as endothelial cells, macrophages, mononuclear cells and smooth muscle cells (SMCs) in atherosclerotic plaques [2,3]. PPARγ is known to regulate these cellular functions including anti-inflammatory and anti-atherogenic actions, as well as inhibitory effects on proliferation and migration of above vascular cells in atheroma [2–5]. In fact, we and others have shown that PPARγ activators reduce the intimal hyperplasia after balloon injury in diabetic models [6], as well as the progression of atherosclerosis in diabetic or hypercholesterolemic models [7,8]. On the other hand, the vascular effects of other activators for PPARs, particularly PPARα, on the vascular cells in vivo remain to be fully elucidated, although the regulatory actions for the macrophages and SMCs have been suggested in vitro [9,10].

* Corresponding author. Tel: +81 43 222 7171x5257; fax: 81 43 226 2095.
E-mail address: hbujo@faculty.chiba-u.jp (H. Bujo).

0021-9150/$ – see front matter © 2004 Elsevier Ireland Ltd. All rights reserved.
doi:10.1016/j.atherosclerosis.2004.08.015

Pioglitazone, a PPARs activator which is world-widely used as an insulin sensitizer for diabetic patients, suppresses carotid intimal thickning accompanied with decreased density of SMC's in intima in diabetic fatty rats [6]. We have shown that the growth and migration activities of SMC's are induced in cultured SMC's isolated from the arteries of diabetic animals compared to normal in vitro [6]. Therefore, the suppression by pioglitazone is largely caused by inhibitory effect on the growth of SMC's, which is resulted from metabolic improvement of diabetes.

TAK-559 is a recently developed, potent activator both for PPARγ and PPARα [11]. The EC50 values for human PPARs activation are 31 nM (γ) and ~67 nM (α), respectively, which concentrations are 16-fold and more than 150-fold lower than those of pioglitazone [12]. Here, we show the inhibitory effect of TAK-559 on the vascular cell recruitment both in vitro and in vivo. Our study using cultured vascular cells, as well as hypercholesterolemic and non-diabetic model, show that the PPARα and γ activator reduces the intimal hyperplasia in hypercholesterolemia, possibly mediated by the inhibitory effects on the recruitment of macrophages and SMC's, independent of the improvement of serum lipid and glucose levels.

2. Materials and methods

2.1. Reagents

Recombinant human TNF-α (hTNF-α), interleukin-1β (IL-1β) and PDGF-BB were purchased from R&D systems (Minneapolis, MN, USA). TAK-559 and pioglitazone were from Takeda Chemical Industries (Osaka, Japan). Rosiglitazone was from GlaxoSmithKline research and Development Limited (Brentford, England). Dulbecco's modified Eagle's medium (DMEM) containing 5.5 mmol/L glucose, Ham's F-12 medium, APMSF and leupeptin were purchased from Sigma Chemical Co. (St. Louis, MS, USA). Fetal bovine serum (FBS) and MCDB medium were from Irvine Scientific (USA) and GIBCO (Tokyo, Japan), respectively.

2.2. Cell culture

THP-1 cells and human umbilical endothelial cells (HUVEC) were obtained from the American Type Culture Collection (Manassas, VA, USA). These cells were maintained in DMEM and Ham's F-12 medium containing 10% FBS, respectively. Primary cultures of rabbit SMC's were prepared from the media of rabbit aorta by the explant method as previously described [13]. Cells from the third to fourth passages were used for experiments. Three different strains of SMC's were used, with similar results. 1 × 105 cells seeded in T-75 flasks were incubated for 48 h in DMEM supplemented in the absence of FBS. For the study of TAK-559, pioglitazone or rosiglitazone on proliferation of SMC's, cell numbers were counted 7 days after adding 10% FBS in the presence or absence of TAK-559, pioglitazone or rosiglitazone, following the incubation without FBS for 48 h.

2.3. Immunohistochemistry

Serial paraffin-embedded sections (10 μm) were used for immunostaining. For immunostaining, we used Pathostain ABC-POD (M) kit (Wako, Tokyo) according to the manufacturer's instructions [14]. The sections were incubated for 5–10 min in 10% H_2O_2 to inactivate endogenous peroxidase. The monoclonal or polyclonal antibody was applied in immunostaining the hydrated sections. Development was with peroxidase-labeled streptavidin and incubation for 30 min in the peroxidase substrate provided. Monoclonal antibodies against rabbit macrophages (RAM11, Dako, Carpinteria, CA) and rabbit smooth muscle α-actin (HHF35, Dako) were used for the identification of rabbit macrophages and SMC's to determine the cell composition of atheromatous plaques, respectively. Hematoxylin was used for counterstaining.

2.4. Adhesion assay

HUVEC were cultured on 60 mm diameter cell culture dishes coated with type I collagen. An hour after IL-1β (1 ng/ml) or TNF-α (10 ng/ml) stimulation, cells were treated with TAK-559 (1 or 10 μM), pioglitazone (10 μM) or rosiglitazone (10 μM) for 24 h. Then THP-1 cells (2×10^5 cells/ml) were added to confluent monolayer HUVEC. After an hour incubation, cells were washed with serum-free MCDB medium and adhering cells were counted by microscopy as previously described [15]. The coefficient of variation using the same sample was less than 0.1%.

2.5. MCP-1 assay

When 80% confluent, the cells were washed and incubated with serum-free MCDB medium for 12 h before being stimulated with 10 ng/ml TNF-α. An hour after TNF-α a stimulation, cells were treated with TAK-559 (1 or 10 μM), pioglitazone (10 μM) or rosiglitazone (10 μM) for 24 h. Cell culture medium were stored at −20 °C for MCP-1 assay by ELISA kit (R&D systems) as described previously [15]. The coefficient of variation using the same sample was less than 0.1%.

2.6. RT-PCR

Total RNA was extracted from the indicated cultured HUVEC as described previously [14]. For RT-PCR, single-stranded cDNA was synthesized from 1 μg of poly(A)+RNA using SuperScript reverse transcriptase (Life Technologies, Tokyo, Japan) and random hexamer primers. One-tenth of the cDNA was subjected to PCR with sense (S) and antisense (AS) primers as follows: 5′-CAGCCAGATGCAATCAATGC-3′ and 5′-

GTGGTCCATGGAATCCTGAA-3′, for human MCP-1; 5′-TCTTCACCACCATGGAGAAGGCTGG-3′ (sense) and 5′-TCCAGGGGTCTTACTCCTTGGAGG-3′ (antisense), for the human GAPDH. The reaction mixture (100 μl) containing the cDNA, 100 pmol of each of the primers, and 2.5 mM dNTP was heated to 95 °C for 10 min, and then immediately cooled on ice. One unit of *Taq* DNA polymerase was added followed by 30 cycles of reannealing at 65 °C for 1 min, elongation at 72 °C for 2 min, and denaturation at 94 °C for 1 min. The PCR products were then analysed on a 2.0% agarose gel and photographed. The relative amount of each signal was determined by densitometric scanning using NIH image™ software. Amounts of MCP-1 mRNA were normalized using the amounts of GAPDH mRNA as reference. The coefficient of variation using the same sample was less than 0.1%.

2.7. Migration

Migration of cells was measured essentially as previously described in a 96-well micro-Boyden chamber (its surface was coated with a type I collagen) [16]. For inhibitory assays, cells were preincubated with TAK-559 (1 or 10 μM), pioglitazone (1 or 10 μM) or rosiglitazone (10 μM) for 48 h at 37 °C, and then aliquots of the cell suspension were added to the upper chamber. The lower chamber contained 1% FBS-DMEM with or without 10 ng/ml PDGF-BB. TAK-559, pioglitazone or rosiglitazone (10 μM) was added to both chambers and were present throughout the experiment. After a 4 h incubation at 37 °C, the cells on the upper surfaces were washed, fixed, and stained by Diff-Quik (International Reagents). The number of cells that migrated to the lower surface of the filters was determined microscopically by counting. The data are presented as "% of increase" of the migrated cell numbers in the absence of PDGF-BB in the lower chambers.

2.8. Animals and experimental atherosclerosis

Japan male white rabbits, 2.5 kg body weight, were used to examine the effect of agents during the process of intimal hyperplasia. These animals were housed in a temperature-, humidity-, and light-controlled room with free access to water. Twelve rabbits were divided to two groups (six rabbit each), and fed with diet (containing agents) for 6 weeks as follows; the first group was fed with atherogenic diet containing 1% cholesterol, and the second group was fed with atherogenic diet containing 1% cholesterol and 0.0066% TAK-559. Two weeks after feeding with atherogenic diet with/without TAK-559, these rabbits were subjected to endothelial denudation of the left common carotid artery using an arterial embolectomy catheter (Fogarty 2F catheter; American Edwards Laboratories, Santa Ana, CA) as described previously [14]. The treated common arteries were removed 4 weeks after endothelial denudation. The common carotid arteries from rabbits after endothelial denudation were used for the following immunohistochemical analysis. Serum TAK-559 concentration was measured by the use of high-performance liquid chromatography/mass spectrometry [11].

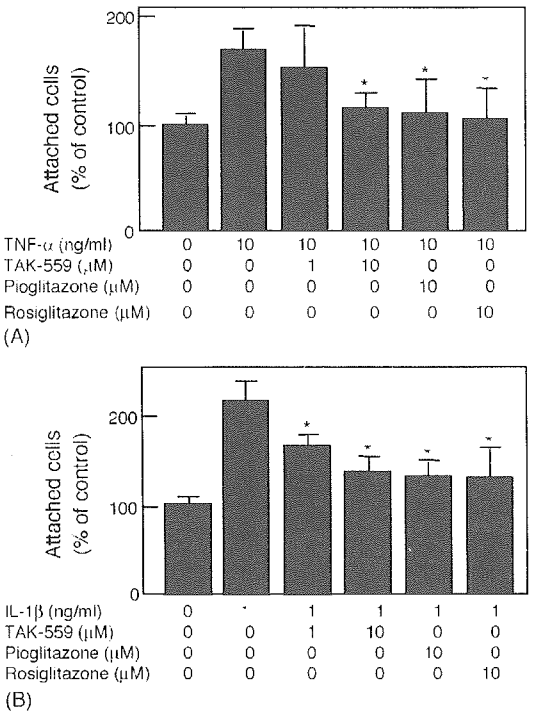

Fig. 1. Effect of TAK-559 on the macrophage adhesion in the cultured endothelial cells. Attached THP-1 cells to HUVEC after the incubation in the presence of TNF-α (A) or IL-1β (B) with without TAK-559 (1 or 10 μM), pioglitazone (10 μM) or rosiglitazone (10 μM). Each value is presented as % of cintrol in the absence of TNF-α (A) or IL-1β (B). Values are means ± S.D. ($n = 3$). $^*P < 0.05$ vs. value in the presence of TNF-α (A) or IL-1β (B) without TAK-559.

2.9. Statistics

The results were shown as mean ± S.D. for each index respectively. Comparison of data were performed using the Student's *t*-test, a value of $P < 0.05$ was considered significant.

3. Results

3.1. Inhibitory effect of TAK-559 on the macrophage recruitment in vitro

In order to know the effect of TAK-559 on macrophage recruitment in vitro, we studied macrophage attachment to endothelial cells, which is known to be important in the process of intimal hyperplasia. As shown in Fig. 1A, TNF-α-induced THP-1 cell attachment to endothelial cells was significantly reduced in the presence of 10 μM

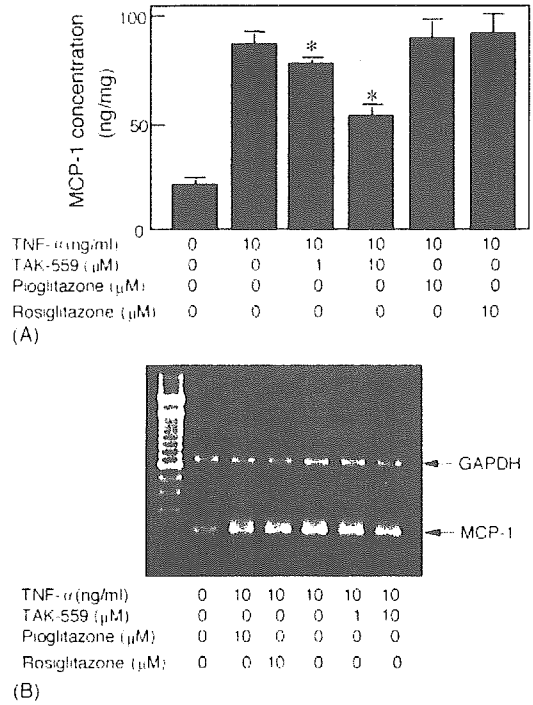

Fig. 2. Effects of TAK-559 on MCP-1 secretion and production in the cultured endothelial cells. (A) Concentration of MCP-1 in the conditioned medium with HUVEC was measured in the presence of TNF-α with without TAK-559 (1 or 10 μM), pioglitazone (10 μM) or rosiglitazone (10 μM). Values are means ± S.D. ($n = 3$). $^*P < 0.05$ vs. value in the presence of TNF-α without TAK-559. (B) Expression of MCP-1 mRNA in HUVEC was evaluated by RT-PCR in the presence of TNF-α with without pioglitazone (10 μM), rosiglitazone (10 μM) or TAK-559 (1 or 10 μM). One-tenth (MCP-1: 110 bp), or 1/50 (GAPDH: 572 bp) of amplified fragments were used for electrophoresis on a 2.0% agarose gel.

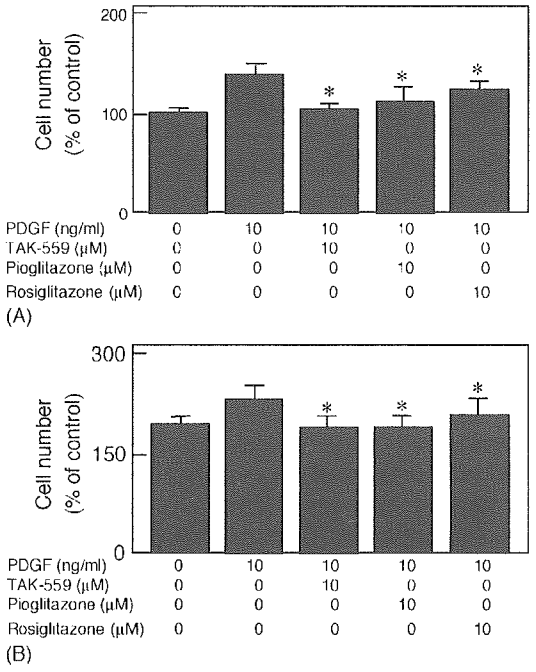

Fig. 3. Effects of TAK-559 on the proliferation and migration of cultured SMCs. (A) Cell numbers 7 days after the incubation with 10 ng/ml PDGF-BB in 1% FBS-DMEM with without TAK-559 (1 μM), pioglitazone (10 μM) or rosiglitazone (10 μM) were measured. Data are represented as % of control. (B) Migration assay was performed using a micro-Boyden chamber. Cells were allowed to migrate at 37 °C for 4 h in the absence or presence of PDGF-BB (10 ng/ml) after the incubation with without TAK-559 (1 μM), pioglitazone (10 μM) or rosiglitazone (10 μM) for 48 h. Then the migrated cells were fixed, stained and counted in the 12 randomly chosen fields of triplicated filters at ×400 magnification. $^*P < 0.05$ vs. value in the presence of PDGF-BB without TAK-559 or pioglitazone.

TAK-559. As shown in Fig. 1B, the IL-1β-induced THP-1 cell attachment to endothelial cells was also significantly reduced in the presence of 1 and 10 μM TAK-559. There was no significant difference of the inhibitory effects (10 μM) among TAK-559, pioglitazone and rosiglitazone.

The several molecule such as adhesion factors and cytokines are known to be involved in the attachment process of macrophage to endothelial cells. Among them, we found the secretion of MCP-1 is affected by the incubation with TAK-559 (Fig. 2). As shown in Fig. 2A, The secretion of MCP-1 from endothelial cells is increased to 4.5-fold in the incubation with TNF-α. The increased secretion of MCP-1 was reversed by 9% and 36% in the presence of 1 and 10 μM TAK-559, respectively, whereas the secretion was not clearly inhibited in the presence of 10 μM pioglitazone or rosiglitazone. Furthermore, RT-PCR analysis showed the effect of TAK-559 on the MCP-1 secretion is accompanied with the reduced mRNA levels in endothelial cells (Fig. 2B). These results indicate that TAK-559 sharply inhibits the synthesis and secretion of MCP-1 from endothelial cells, possibly contributing the decreased attachment of macrophages to endothelial cells in culture system.

3.2. TAK-559 inhibits the proliferation and migration of SMCs

We next examined the effect of TAK-559 on the proliferation and migration of SMC's. The proliferation of SMCs 7 days after the incubation with serum was significantly decreased in the cells in the presence of TAK-559 as well as pioglitazone and rosiglitazone (Fig. 3A). The PDGF-induced migration activity was also decreased in the presence of TAK-559 (Fig. 3B). These results show that TAK-559 has inhibitory effects on the proliferation and migration of SMCs in addition to the effects on the macrophage recruitment.

3.3. Effects of TAK-559 on the carotid intimal thickness of hypercholesterolemic rabbits

The rabbits were divided to two groups (six each), and each group was administrated with 1% cholesterol diet (control), or 1% cholesterol diet containing TAK-559. Balloon catheterization was performed using left carotid artery 2 weeks after the administration with each diet with or without agents. The histological findings of injured arteries and plasma levels of lipid glucose and insulin were analysed 4 weeks after bal-

Table 1
Plasma lipid, glucose and insulin levels of rabbits after ballooning injury

	Control	TAK-559	*P*-value
TC (mg/dl)	1477 ± 276	1301 ± 370	ns
TG (mg/dl)	80 ± 59	64 ± 71	ns
HDL-C (mg/dl)	32 ± 28	50 ± 22	ns
Insulin (ng/ml)	0.32 ± 0.13	0.31 ± 0.09	ns

loon injury. The averaged body weights of rabbits 4 weeks after balloon catheterization shows no significant difference between control rabbits and TAK-559-treated rabbits (2.9 ± 0.2 kg versus 2.8 ± 0.3 kg). As shown in Table 1, plasma total cholesterol level showed the severe hypercholesterolemia both in two groups. The cholesterol levels, as well as triglyceride, glucose and insulin levels, were not significantly different between these two groups.

Fig. 4A shows that the sections of carotid arteries from rabbits administrated with 1% cholesterol diet or 1% cholesterol diet containing TAK-559, 4 weeks after balloon injury. There were obvious intimal hyperplasia consisted of abundant mononuclear cells as well as intracellular matrices and accumulated lipids in the sections from rabbits administrated with 1% cholesterol diet. The sections of arteries from TAK-559-treated rabbits shows less thickened intimal layers compared with sections from rabbits administrated with 1% cholesterol diet. The changes in the I/M ratio are shown in Fig. 4B. Compared to the I/M ratio of the sections from in control rabbits fed with 1% cholesterol diet, the ratio of sections from rabbits fed with 1% cholesterol diet containing TAK-559 showed that significant decrease by 51% ($P < 0.05$). These findings indicate that TAK-559 appears to have an inhibitory effect on the intimal thickning induced by balloon catheterization.

We next performed immunohistochemical staining of neighbouring slices for the identification of vascular mononuclear cells (Fig. 5A). There were drastic decreases in the sections stained for macrophages, and slight decreases in SMCs. Fig. 5B shows the cell numbers of macrophages (a) and SMCs (b) in intima. The number of macrophage was decreased to 34% in the intima in the slices from TAK-559-treated rabbits compared to the slices from control rabbits. The number of SMCs was also significantly decreased to 49% in the intima in the slices from TAK-559-treated rabbits, compared to the slices from control rabbits. These results indicate that the reduced thickness in intima in the TAK-559-treated rabbits is accompanied with reduced recruitment of macrophages and SMCs in hyperplastic intima.

4. Discussion

In this study, we identified the effects of a newly developed dual PPARs agonist, TAK-559, on the vascular cell recruitment in vitro and the intimal thickning by the balloon catheterization using hypercholesterolemic, non-diabetic rabbits. The potent agonist both for PPARα and PPARγ showed the strong inhibition of intimal hyperplasia, although the plasma lipids, glucose and insulin levels were not changed min the rabbits. The inhibitory effect was thought to be caused by the strong inhibition of macrophage recruitment as well as the inhibition of proliferation and migration of SMCs, based on the inhibitory effects on the recruitment of vascular cells observed in vitro. These results suggest that the potent PPARs dual agonist reduces the intimal hyperplasia followed by the endothelial denudation in the presence of hypercholestrolemia, but not glucose intolerance.

Recent in vivo studies suggest that PPAR activators limit experimental atherosclerosis in animal models [17,18]. Notably, PPARγ ligands inhibit development of atherosclerosis in non-diabetic, in addition to diabetic, LDL receptor-deficient mice [7,8]. PPARγ-specific agonists, Rosiglitazone and GW7845 inhibit the development of atherosclerosis in LDL receptor-deficient mice, and it was suggested to correlated with local actions of PPARγ, such as decreased expres-

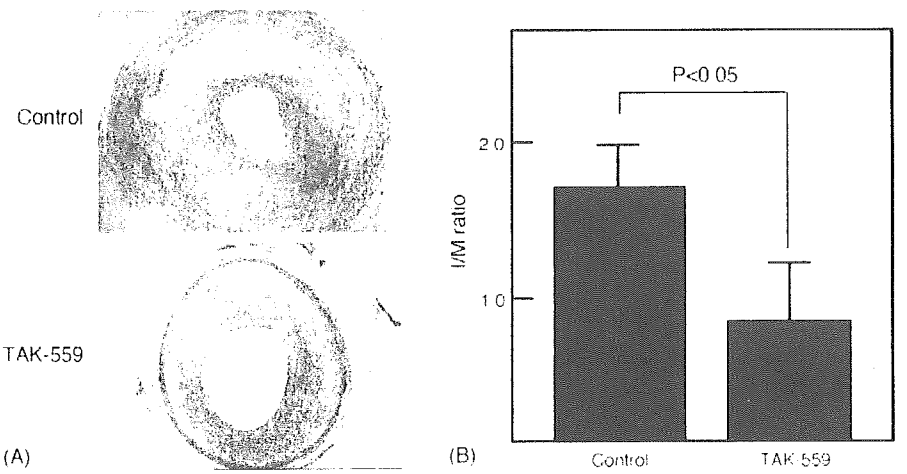

Fig. 4. Effect of TAK-559 on the intimal thickning of carotid arteries after balloon injury in hypercholesterolemic rabbits. (A) Carotid artery sections stained with Hematoxilin–Eosin. The section of arteries from rabbits fed with atherogenic diet containing 1% cholesterol (control), or with atherogenic diet containing 1% cholesterol 0.0066% TAK-559 (TAK-559), 4 weeks after balloon injury, is shown. (B) I/M ratio of carotid arteries. Data are mean ± S.D. ($n = 6$).

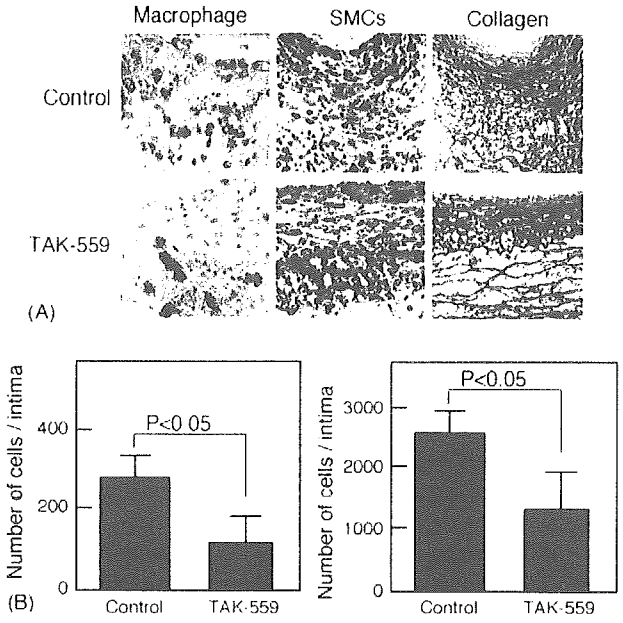

Fig. 5. Macrophages, SMCs and collagen fibrils in the intimal thickning of carotid arteries after balloon injury in hypercholesterolemic rabbits. (A) Carotid artery sections were immunostained with antibody against macrophages or smooth muscle alpha-actin, or stained with Elastica-Masson. The sections of arteries from rabbits fed with atherogenic diet containing 1% cholesterol (control), with atherogenic diet containing 1% cholesterol and 0.0066% TAK-559 (TAK-559), 4 weeks after balloon injury, are shown. (B) Cell numbers of immunologically identified macrophage (a) and SMCs (b) in the hyperplastic intima in the sections of carotid arteries from rabbits fed with atherogenic diet containing 1% cholesterol (control), or with atherogenic diet containing 1% cholesterol and 0.0066% TAK-559 (TAK-559), 4 weeks after balloon injury, are shown. Data are mean ± S.D. ($n = 6$).

sion of TNF-α and gelatinase B [8]. These drugs are highly specific for PPARγ with EC50 of 76 nM and 1.2 nM, respectively, and not for PPARα (EC50 both in excess of 10 μM). Another PPARγ-specific agonist, troglitazone inhibits lesion formation in non-diabetic, as well as diabetic LDL receptor-deficient mice accompanied with significant decrease of accumulation of lesional macrophages [7]. These studies have revealed the direct effects of PPARγ activation in the artery wall, particularly on the recruitment of macrophages.

The in vivo inhibitory effects of PPARs on the proliferation and migration of SMCs were identified by us and others [6,17,18]. Troglitazone significantly reduces arterial neointimal hyperplasia after endothelial injury in rats [19]. Pioglitazone has shown to suppress the neointimal formation after arterial injury using air-drying method [20]. In this model, there were no significant differences between pioglitazone-treated and control rats in plasma glucose and insulin levels. We have shown that pioglitazone decreases SMCs density of carotid arterial intima after balloon catheterization in obese-hyperglycemic rat [6]. The inhibitory effects of pioglitazone were thought to be largely caused by the improvement of plasma lipid, glucose and insulin levels. However, the following characterization of an inhibitory effect of pioglitazone on balloon-induced SMCs growth in non-diabetic rats uncovered the possible local effects of agent on the growth of SMCs [21]. The inhibitory effects of TAK-559 on the proliferation and migration of SMCs seem to be in agreement with these previous in vivo studies.

The local effect in vascular wall is possibly caused by the function of PPARα and PPARγ as anti-inflammatory mediators in atheroma-associated cells. PPARγ is expressed in endothelial cells, macrophages, mononuclear cells and SMCs in the aortic intima, and PPARα is co-expressed with PPARγ in some of these cells [2,3]. In vitro experiments demonstrate that PPARα and PPARγ activators decrease inflammatory proteins, such as adhesion molecules, cytokines, and chmokines, in macrophages, endothelial cells, lymphocytes and SMCs [2–5,9,10,22–24]. In addition to accumulating evidence of local actions of PPARγ in arterial walls, our study might show the possibility of actions of PPARγ, or combined effects of PPARα and PPARγ, on the reduced recruitment of macrophages and SMCs. A currently available PPARs activator, pioglitazone, despite a lower binding affinity to PPARγ, is more potent than BRL, a PPARγ agonist, in inhibiting IFN-γ protein production [25]. This is possibly due to the combined PPARα and PPARγ effect observed in pioglitazone, given that this agent (in contrast to BRL) can also activate PPARα. This study shows that such a potent activity for PPARα in addition to PPARγ might contribute the inhibitory action for the intimal thickness in hypercholesterolemic model. In contrast, PPARγ itself is known to activate the CD36 scavenger receptor on macrophage [26,27]. In this context, PPARα might reduce the lipid accumulation in macrophages because of the enhancement of the availability of free cholesterol for efflux through the ABCA1 pathway [10]. In our hypercholesterolemic model, the enhanced lipid accumulation in macrophages was not observed in the intima from TAK-559-treated mice. The PPAR activation with pioglitazone prevents coronary arteriosclerosis in rat inflammation model with L-NAME through downregulation of the MCP-1 receptor in lesional and circulating monocytes [22,28]. TAK-559 showed the inhibition of macrophage attachment and MCP-1 secretion in vitro. Notably the effects of MCP-1 production and secretion of TAK-559 were obvious among the in vitro effects studied here compared to pioglitazone and rosiglitazone. The inhibitory effects of TAK-559 on MCP-1 might be contributed by the potent PPARα activation in addition to PPARγ activation. Thus, the combined PPARα and γ-mediated actions might influence the recruitment of macrophages through lipid accumulation and MCP-1 secretion in macrophages after balloon injury in hypercholesterolemic model.

In summary, we identified the inhibitory effects of potent agonist both for PPARα and PPARγ, TAK-559, on the vascular cell recruitment and intimal thickning by the balloon catheterization using hypercholesterolemic, non-diabetic rabbits. The strong inhibition of intimal hyperplasia by TAK-559 was observed although the serum lipid and insulin levels were not obviously changed. The inhibitory effect

was thought to be caused by the inhibition of macrophage recruitment as well as the inhibition of proliferation and migration of SMC's. These results suggest that the vascular effects of PPAR agonists can be expected to protect the progress of intimal thickning in hyperlipidemic patients, in addition to the metabolic effects on the insulin-resistant state in the diabetic patients. Further molecular analyses for the identification of inhibitory effects of TAK-559 on the recruitment of macrophages and SMC's, particularly the potent effect on the MCP-1 secretion, are needed to know the drastic in vivo inhibitory effects on the intimal thickning in hypercholesterolemic model.

Acknowledgements

These studies were supported by grants from the Japanese Ministry of Education, Culture, Sports, Science and Technology to Y.S. and H.B. We thank Drs. M. Igarashi (Yamagata Univ.) and A. Haruno (Taiho Pharmacological Co.) for the instruction of balloon catheterization method. The authors are grateful to Takeda Chemical Industries, Ltd. for the supply of TAK-559 and pioglitazone, and for valuable suggestions. The authors are also grateful to GlaxoSmithKline for the supply of Rosiglitazone.

References

[1] Hsueh WA, Law RE. PPARγ and atherosclerosis: effects on cell growth and movement. Arterioscler Thromb Vasc Biol 2001;21:1891–5.
[2] Ricote M, Huang J, Fajas L, et al. Expression of the peroxisome proliferator-activated receptor gamma (PPAR-γ) in human atherosclerosis and regulation in macrophages by colony stimulating factors and oxidized low-density lipoprotein. Proc Natl Acad Sci USA 1998;23:7614–9.
[3] Law RE, Goetz S, Xi XP, et al. Expression and function of PPAR-γ in rat and human vascular smooth muscle cells. Circulation 2000;101:1311–8.
[4] Kwak BR, Myit S, Mulhaupt F, et al. PPARgamma but not PPARalpha ligands are potent repressors of major histocompatibility complex class II induction in atheroma-associated cells. Circ Res 2002;90(22):356–62.
[5] Calnek DS, Mazzella L, Roser S, Roman J, Hart CM. Peroxisome proliferator-activated receptor gamma ligands increase release of nitric oxide from endothelial cells. Arterioscler Thromb Vasc Biol 2003;23:52–7.
[6] Igarashi M, Takeda Y, Ishibashi N, et al. Pioglitazone reduces smooth muscle cell density of rat carotid arterial intima induced by balloon catheterization. Horm Metab Res 1997;29:444–9.
[7] Collins AR, Meehan WP, Kintscher U, et al. Troglitazone inhibits formation of early atherosclerotic lesions in diabetic and nondiabetic low density lipoprotein receptor-deficient mice. Arterioscler Thromb Vasc Bio 2001;21:365–71.
[8] Li AC, Brown KK, Silvestre MJ, et al. Peroxisome proliferator-activated receptor gamma ligands inhibit development of atherosclerosis in LDL receptor-deficient mice. J Clin Invest 2000;106:523–31.
[9] Kintscher U, Lyon C, Wakino S, et al. PPARalpha inhibits TGF-beta-induced beta5 integrin transcription in vascular smooth muscle cells by interacting with Smad4. Circ Res 2002;91:35–44.
[10] Chinetti G, Lestavel S, Fruchart JC, Clavey V, Staels B. Peroxisome proliferator-activated receptor alpha reduces cholesterol esterification in macrophages. Circ Res 2003;92:212–7.
[11] Imoto H, Sugiyama Y, Kimura H, Momose Y. Studies on non-thiazolidinedione antidiabetic agents. 2. Novel oxyiminoalkanoic acid derivatives as potent glucose and lipid lowering agents. Chem Pharm Bull (Tokyo) 2003;51:138–51.
[12] Sakamoto J, Kimura H, Moriyama S, et al. Activation of human peroxisome proliferator-activated receptor (PPAR) subtypes by pioglitazone. Biochem Biophys Res Commun 2000;278:704–11.
[13] Zhu Y, Bujo H, Yamazaki H, et al. Enhanced expression of the LDL receptor family member LR11 increases migration of smooth muscle cells in vitro. Circulation 2002;105:1830–6.
[14] Kanaki T, Bujo H, Hirayama S, et al. Expression of LR11, a mosaic LDL receptor family member, is markedly increased in atherosclerotic lesions. Arterioscler Thromb Vasc Biol 1999;19:2687–95.
[15] Yokote K, Morisaki N, Zenibayashi M, et al. The phospholipase-A2 reaction leads to increased monocyte adhesion of endothelial cells via the expression of adhesion molecules. Eur J Biochem 1993;217:723–9.
[16] Zhu Y, Bujo H, Yamazaki H, et al. LR11, an LDL receptor gene family member, is a novel regulator of smooth muscle cell migration. Circ Res 2004, Epub ahead of print.
[17] Rosen ED, Spiegelman BM. Peroxisome proliferator-activated receptor gamma ligands and atherosclerosis: ending the heartache. J Clin Invest 2000;106:629–31.
[18] Glass CK. Antiatherogenic effects of thiazolidinediones? Arterioscler Thromb Vasc Biol 2001;21:295–6.
[19] Law RE, Meehan WP, Xi XP, et al. Troglitazone inhibits vascular smooth muscle cell growth and intimal hyperplasia. J Clin Invest 1996;98:1897–905.
[20] Yoshimoto T, Naruse M, Shizume H, et al. Vasculo-protective effects of insulin sensitizing agent pioglitazone in neointimal thickening and hypertensive vascular hypertrophy. Atherosclerosis 1999;145:333–40.
[21] Igarashi M, Hirata A, Yamaguchi H, et al. Characterization of an inhibitory effect of pioglitazone on balloon-injured vascular smooth muscle cell growth. Metabolism 2001;50:955–62.
[22] Ishibashi M, Egashira K, Hiasa K, et al. Antiinflammatory and antiarteriosclerotic effects of pioglitazone. Hypertension 2002;40:687–93.
[23] Xin X, Yang S, Kowalski J, Gerritsen ME. Peroxisome proliferator-activated receptor gamma ligands are potent inhibitors of angiogenesis in vitro and in vivo. J Biol Chem 1999;274:9116–21.
[24] Yoshimoto T, Naruse M, Shizume H, et al. Vasculo-protective effects of insulin sensitizing agent pioglitazone in neointimal thickening and hypertensive vascular hypertrophy. Atherosclerosis 1999;145:333–40.
[25] Marx N, Kehrle B, Kohlhammer K, et al. PPAR activators as anti-inflammatory mediators in human T lymphocytes: implications for atherosclerosis and transplantation-associated arteriosclerosis. Circ Res 2002;90:703–10.
[26] Nagy L, Tontonoz P, Alvarez JG, Chen H, Evans RM. Oxidized LDL regulates macrophage gene expression through ligand activation of PPARgamma. Cell 1998;93:229–40.
[27] Tontonoz P, Nagy L, Alvarez JG, Thomazy VA, Evans RM. PPAR gamma promotes monocyte macrophage differentiation and uptake of oxidized LDL. Cell 1998;93:241–52.
[28] Egashira K. Molecular mechanisms mediating inflammation in vascular disease: special reference to monocyte chemoattractant protein-1. Hypertension 2003;41:834–41.

Original Article

Angiotensin II Type 1 Receptor Antagonist and Angiotensin-Converting Enzyme Inhibitor Altered the Activation of Cu/Zn-Containing Superoxide Dismutase in the Heart of Stroke-Prone Spontaneously Hypertensive Rats

Masakazu TANAKA, Seiji UMEMOTO*, Shinji KAWAHARA, Makoto KUBO, Shinichi ITOH, Kyoko UMEJI, and Masunori MATSUZAKI

Although angiotensin II type 1 (AT1) receptor antagonists and angiotensin-converting enzyme (ACE) inhibitors are known to reduce both reactive oxygen species (ROS) generated by activated NAD(P)H oxidase and vascular remodeling in hypertension, the effects of AT1 receptor antagonists or ACE inhibitors on ROS-scavenging enzymes remain unclear. We hypothesized that AT1 receptor antagonists or ACE inhibitors may modulate vascular remodeling *via* superoxide dismutase (SOD) in hypertension. Male stroke-prone spontaneously hypertensive rats (SHRSP) were treated for 6 weeks with a vehicle, an AT1 receptor antagonist (E4177; 30 mg/kg/day), or an ACE inhibitor (cilazapril; 10 mg/kg/day). We evaluated protein expression using immunoblots, determined SOD activities with a spectrophotometric assay, and measured NAD(P)H oxidase activity by a luminescence assay. The two drugs showed equipotent effects on blood pressure, left ventricular hypertrophy and fibrosis, and endothelial NO synthase in the SHRSP hearts. The wall-to-lumen ratio of the intramyocardial arteries and the NAD(P)H oxidase essential subunit $p22^{phox}$ and its activity were significantly reduced, whereas Cu/Zu-containing SOD (Cu/ZnSOD) expression and activity were significantly increased in the SHRSP hearts. Furthermore, E4177 reduced vascular remodeling more than did cilazapril not only by reducing $p22^{phox}$ expression and NAD(P)H oxidase activity but also by upregulating the Cu/ZnSOD expression and its activity in the SHRSP hearts. Thus, both the AT1 receptor antagonist and the ACE inhibitor inhibited vascular remodeling and reduced ROS in SHRSP *via* not only a reduction in NAD(P)H oxidase but also an upregulation of Cu/ZnSOD. (*Hypertens Res* 2005; 28: 67–77)

***Key Words*: superoxide dismutase, angiotensin, vascular remodeling, stroke-prone spontaneously hypertensive rats, oxidative stress**

Introduction

Increased production of vascular reactive oxygen species (ROS), especially superoxide anion, contributes to functional and structural alterations in hypertension. By stimulating the angiotensin II (Ang II) type 1 (AT1) receptor, Ang II contributes to the overexpression of cytosolic proteins involved in the activation of NAD(P)H oxidase, which is a major source of superoxide production (*1, 2*). Overexpression of these

From the Department of Cardiovascular Medicine, Yamaguchi University Graduate School of Medicine, Ube, Japan; and *Pharmaceutical Clinical Research Center, Yamaguchi University Hospital, Ube, Japan.

This study was supported in part by grants from Eisai Co., Ltd. and the Takeda Science Foundation.

Address for Reprints: Masunori Matsuzaki, M.D., Ph.D., Department of Cardiovascular Medicine, Yamaguchi University Graduate School of Medicine, 1–1–1 Minamikogushi, Ube 755–8505, Japan. E-mail: masunori *a* yamaguchi-u.ac.jp

Received March 10, 2004; Accepted in revised form September 30, 2004.

cytosolic proteins might lead to vascular hypertrophy and remodeling in hypertension (*1*, *2*), and the AT1 receptor antagonist reduces overall oxidative stress in hypertensive patients independently of its effects on blood pressure (*3*). Conversely, enzyme superoxide dismutase (SOD) is a primary cellular defense against ROS. Three SOD isozymes, Cu/Zu-containing SOD (Cu/ZnSOD), manganese SOD (MnSOD), and extracellular SOD (ecSOD), have been identified, with Cu/ZnSOD being localized in the cytosol, MnSOD in mitochondria, and ecSOD in extracellular spaces. The predominant SOD activity in rat peripheral vessels is attributed to Cu/ZnSOD (*4*, *5*). Exposure to oxidative stress induced by the activation of NAD(P)H oxidase may exhaust the antioxidative capacity of the heart. In contrast, the increased activity of NAD(P)H oxidase is attenuated by increased activation of SOD induced by the administration of antioxidants in stroke-prone spontaneously hypertensive rats (SHRSP) (*6*), indicating that upregulation of antioxidant enzymes might reduce oxidative stress, improve vascular function and structure, and prevent the progression of hypertension in SHRSP.

Despite the many studies on the beneficial effects of angiotensin-converting enzyme (ACE) inhibitors and AT1 receptor antagonists on the vascular structure of intramyocardial arteries and oxidative stress in hypertension (*1*, *2*), the effects of AT1 receptor antagonists and ACE inhibitors on ROS-scavenging enzymes remain unclear. In this study, we assessed the hypothesis that AT1 receptor antagonists or ACE inhibitors might modulate vascular remodeling in the intramyocardial arteries of SHRSP *via* ROS-scavenging enzymes such as SOD.

Methods

The Ethics Committee for Animal Experimentation at the Yamaguchi University School of Medicine approved the experimental protocol used in this study. Experiments were performed according to the Guidelines for Animal Experimentation at the Yamaguchi University School of Medicine, and according to law No. 105 and notification No. 6 of the Japanese government.

Chemicals and Antibodies

The AT1 receptor antagonist E4177 and the ACE inhibitor cilazapril were provided by Eisai Co., Ltd. (Tokyo, Japan). The following were used in the immunofluorescence study and immunoblots: mouse monoclonal antibodies against human α-smooth muscle (SM) actin (Dako Cytomation Co., Ltd., Kyoto, Japan), human MnSOD (Chemicon International, Temecula, USA), human endothelial NO synthase (eNOS) (BD Transduction Laboratories, San Diego, USA), goat polyclonal antibodies against human $p22^{phox}$, Cu/ZnSOD, and calponin-1 (Santa Cruz Biotech, Santa Cruz, USA), horseradish peroxidase (HRP)-rabbit anti-goat and anti-mouse IgG, FITC-conjugated rabbit anti-mouse IgG (Zymed Laboratories, San Francisco, USA), and TRITC-conjugated rabbit anti-goat IgG (P.A.R.I.S., Compiègne, France).

Experimental Protocol

Twelve-week-old male Wistar-Kyoto rats (WKY group; $n = 20$) and SHRSP ($n = 60$) were obtained from Charles River Japan (Yokohama, Japan). SHRSP were randomized into three groups and treated for 6 weeks with a vehicle (SHRSP group; $n = 20$), cilazapril (10 mg/kg/day, cilazapril group; $n = 20$), or E4177 (30 mg/kg/day, E4177 group; $n = 20$). The doses used in the experiments were determined according to Matsumoto *et al.* (*7*). Without anesthetizing the rats, we determined their systolic blood pressure (SBP) and heart rate by tail-cuff plethysmography. After the 6-week treatment period, rats were weighed and euthanized with a sodium pentobarbital overdose, and hearts were excised and weighed. Some of the excised hearts were perfused and fixed with heparinized saline followed by Bouin's solution *via* retrograde infusion into the ascending aorta at a pressure of 90 mmHg (*8*), and then paraffin-embedded 4-μm slices were stained with Sirius red for histological analysis. The left ventricles of the other hearts were separated, washed with heparinized saline, weighed, and cut into three pieces perpendicular to the long axis. A piece of the middle portion of the heart tissue from each heart was snap-frozen with optimal cutting temperature (O.C.T.) compound in liquid nitrogen to obtain fresh-frozen, 4-μm-thick sections for immunofluorescent staining. The rest of the apex-side heart tissues were frozen in liquid nitrogen and stored at −80°C until use for immunoblotting. The remaining base-side heart tissues were not used for the study, as we wanted to avoid contaminating the epicardial large coronary arteries.

Histological Analysis

To evaluate the coronary arterial wall thickness and perivascular fractional fibrosis, we scanned short-axis images of intramyocardial arteries at ×200 magnification. In each heart, we evaluated the wall-to-lumen ratio (the medial thickness compared to the internal diameter) and a cross-sectional area of at least 10 intramyocardial arteries < 150 μm in diameter, as well as the perivascular collagen (the ratio of the collagen deposition area surrounding the vessel to the lumen area) and the interstitial collagen fraction (the ratio of the collagen deposition area in interstitial spaces and the corresponding left ventricular area) in the heart by analyzing Sirius red-stained sections under a microscope fitted with cross-polarization filters. All were evaluated in a blind fashion using a computer-assisted image analysis system with NIH Image software (ver. 1.62), according to the method of Baba *et al.* (*9*), and the mean value of each heart was used for statistical analysis.

Confocal Microscopy

We conducted dual immunolabeling using combinations of mouse monoclonal antibody against α-SM actin (dilution 1:100) and goat polyclonal antibodies against $p22^{phox}$ (dilution 1:100) or Cu/ZnSOD (dilution 1:100), or goat polyclonal antibodies against calponin-1 (dilution 1:50) and mouse monoclonal antibodies against MnSOD (dilution 1:200), to evaluate the colocalization of these proteins. After fixation, the sections were treated with 2.0% normal horse and 5.0% normal sheep serum (Vector Laboratories, Burlingame, USA) in phosphate-buffered saline for 30 min at room temperature, followed by incubation overnight at 4 C with the two primary antibodies applied together. The sections were then incubated for 1 h at room temperature with a mixture of the two secondary antibodies, FITC-conjugated rabbit anti-mouse IgG (dilution 1:100 or 200) and TRITC-conjugated rabbit anti-goat IgG (dilution 1:100). The sections were washed with three changes of phosphate-buffered saline, mounted in glycerol, and then examined by confocal microscopy with a laser scanning confocal fluorescence microscope (LSM510; Carl Zeiss, Inc., Jena, Germany) equipped with argon and helium-neon laser sources. Excitation wavelengths of 488 nm for FITC and 543 nm for TRITC were used to generate fluorescence emissions in green and red, respectively.

Immunoblotting

Immunoblots were performed as previously described (*10*). The $p22^{phox}$, Cu/ZnSOD, and MnSOD were separated by sodium dodecyl sulfate (SDS) -15% polyacrylamide gel electrophoresis (PAGE), and eNOS was separated on SDS-10% PAGE. Primary antibodies against $p22^{phox}$ and Cu/ZnSOD were used at a dilution of 1:500; MnSOD and eNOS were used at a dilution of 1:1000. Equal amounts of protein of total tissue homogenate from heart tissue were applied in each well ($p22^{phox}$, 40 μg; Cu/ZnSOD, 30 μg; MnSOD, 12 μg; eNOS, 20 μg) and then electroblotted and detected with the ECL system (Amersham Biosciences, Buckinghamshire, UK). After immunoblotting, the film was scanned and densitometric analyses were performed using NIH Image software (ver. 1.62).

Measurement of Oxidative Stress

Myocardial oxidative stress was estimated by measuring both 8-*iso*-prostaglandin $F_{2\alpha}$ (8-*iso*-$PGF_{2\alpha}$) and thiobarbituric acid reactive substances (TBARS). The level of 8-*iso*-$PGF_{2\alpha}$ was measured using an enzyme-linked immunoassay kit (Cayman Chemicals, Ann Arbor, USA) (*11*). Briefly, cardiac tissues were homogenized and then protected by the addition of indomethacin (0.001% w/v) to prevent *in vitro* formation of prostanoids due to any leukocyte contamination. Tissues were hydrolyzed with the appropriate excess volume of 2 mol/l KOH at 45 C for 2 h. After hydrolysis, samples were cooled and treated with an equal volume of 2 mol/l HCl, and the neutralized samples were then centrifuged at 3,000 rpm for 20 min. Using 8-*iso*-$PGF_{2\alpha}$ as the standard, we calculated the level of 8-*iso*-$PGF_{2\alpha}$ as pg/mg wet tissue.

TBARS levels were determined by a colorimetric method (Wako Pure Chemicals, Tokyo, Japan) (*12*). Briefly, cardiac tissue was homogenized in 6.5% trichloroacetic acid (TCA), and a reagent containing 15% TCA, 0.375% thiobarbituric acid, and 0.25% HCl was added. The sample was then mixed thoroughly, heated for 15 min in a boiling water bath, cooled, and centrifuged at 2,000 rpm; the absorbance of the supernatant was then measured at 535 nm against a blank that contained all reagents except the tissue homogenate. Using malondialdehyde as a standard, we calculated TBARS as nmol/mg wet tissue.

Measurement of SOD Activity

SOD activities were determined based on the SOD-mediated increase in the rate of autoxidation of 5,6,6a,11b-tetrahydro-3,9,10-trihydroxybenzo[c]fluorine in aqueous alkaline solution to yield a chromophore with maximum absorbance at 525 nm with a spectrophotometric assay (OxisResearch, Portland, USA) (*13*). Briefly, heart tissues were washed with 0.9% NaCl containing heparin to remove red blood cells, followed by homogenization and centrifugation. Next, 40 μl of tissue homogenate was added to 900 μl of 2-amino-2-methyl-1,3-propanediol containing boric acid and diethylenetriaminepentaacetic acid (DTPA) (pH 8.8), and then 30 μl of 1,4,6-trimethyl-2,2-vinylpyridinium trifluoromethanesulfonate in HCl was added. The mixture was briefly vortexed and then incubated at 37 C for 1 min. We added 30 μl of 5,6,6a,11b-tetrahydro-3,9,10-trihydroxybenzo[c]fluorine in HCl containing DTPA and ethanol, and immediately measured the absorbance at 525 nm spectrophotometrically. The SOD activity was determined from the ratio of the autoxidation rates in the presence and absence of SOD. Absolute ethanol/chloroform, 62.5/37.5 (v/v), was used to inactivate MnSOD and to specifically measure Cu/ZnSOD activity according to the manufacturer's recommendations.

Measurement of NAD(P)H Oxidase Activity

NAD(P)H oxidase activities were determined by a luminescence assay (*14*). Briefly, heart tissues were placed in a chilled, modified Krebs-HEPES buffer (99 mmol/l NaCl, 4.7 mmol/l KCl, 1.9 mmol/l $CaCl_2$, 1.2 mmol/l $MgSO_4$, 1.0 mmol/l K_2HPO_4, 25 mmol/l $NaHCO_3$, 20 mmol/l Na-HEPES, and 11 mmol/l glucose, pH 7.4). A 10% (w/v) tissue homogenate in a 50 mmol/l phosphate buffer was subjected to centrifugation at 1,000×*g* for 10 min to remove unbroken cells and debris. An aliquot was kept for protein determination, and supernatants (25 μl) were assayed immediately for superoxide production. A luminescence assay was performed in a 50 mmol/l phosphate buffer, pH 7.0, containing 1 mmol/l

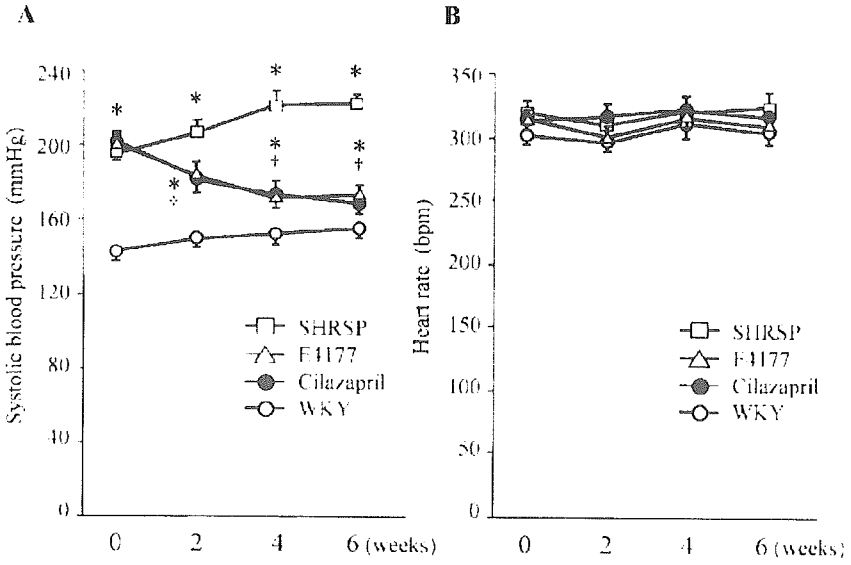

Fig. 1. *Systolic blood pressure and heart rate in the WKY, vehicle SHRSP, cilazapril, and E4177 groups. Bars indicate SEM.* *p < *0.01* vs. *the WKY group.* †p < *0.01* vs. *the vehicle SHRSP group. Experiments,* n = *5–7.*

EGTA, 150 mmol/l sucrose, 500 μmol/l lucigenin (bis-*N*-methylacridinium nitrate) as the electron acceptor, and 100 μmol/l NAD(P)H as the substrate (final volume 225 μl), all of which was poured into a 96-well microplate. This concentration fell well within the linear range of the assay (1 μmol/l to 10 mmol/l for NAD(P)H), and NAD(P)H was not rate-limiting over the initial course of the assay. No activity could be measured in the absence of NAD(P)H. After dark adaptation, background counts were recorded and a tissue homogenate was added to the microplate. The lucigenin count was then recorded every 15 s for 10 min, and the respective background counts (without tissue homogenate) were subtracted from tissue homogenate readings. The lucigenin count was expressed as counts per second per milligram of the tissue homogenate.

Statistical Analysis

All values were expressed as the means±SEM. The experimental groups were compared with ANOVA followed by Scheffe's multiple comparisons; values of $p<0.05$ were considered statistically significant.

Results

Throughout the experiments, SBP in the vehicle SHRSP group was significantly higher than that in the WKY group. The two drugs induced equivalent and significant reductions in SBP compared to the levels in the SHRSP group. However, both the cilazapril and E4177 groups showed significantly higher SBP than did the WKY group (Fig. 1A). Heart rates were unaltered among the four groups throughout the experiments (Fig. 1B). Body weight was greater in the WKY group than in the three SHRSP groups, but there was no difference in body weight among the three SHRSP groups. Left ventricular weight/body weight in the three SHRSP groups was significantly greater than that in the WKY group. In addition, compared to the vehicle SHRSP group, the two drug-treated SHRSP groups showed significant and equal reductions in left ventricular weight/body weight (Table 1).

Table 1. BW and LVW in 18-Week-Old Rats

Parameter	WKY	SHRSP	Cilazapril	E4177
BW (g)	389±11	295±5*	293±4*	297±4*
LVW (mg)	843±13	857±14	768±15*,†	735±10*,†
LVW/BW (mg/g)	2.07±0.1	2.76±0.1*	2.48±0.1*,‡	2.38±0.1*,‡

Values are the mean±SEM. WKY and SHRSP were treated with vehicle, cilazapril (10 mg/kg/day), or E4177 (30 mg/kg/day) for 6 weeks. *$p<0.01$ *vs.* the WKY groups, †$p<0.01$, ‡$p<0.05$ *vs.* the SHRSP group. BW, body weight; LVW, left ventricular weight; WKY, Wistar-Kyoto rats; SHRSP, stroke-prone spontaneously hypertensive rats. Experiments, $n=8$.

Figure 2 shows a representative micrograph of the effects of cilazapril and E4177 on vascular remodeling and perivascular collagen deposition in an intramyocardial artery, and Table 2 summarizes the quantitative analysis of the wall-to-lumen ratio and the cardiac collagen deposition in rat hearts. The wall-to-lumen ratio and cross-sectional area of the intramyocardial arteries in the vehicle SHRSP group were significantly greater than those in the WKY group. Both these parameters were significantly lower in the two drug-treated groups than in the vehicle SHRSP group. Furthermore, E4177 reduced the

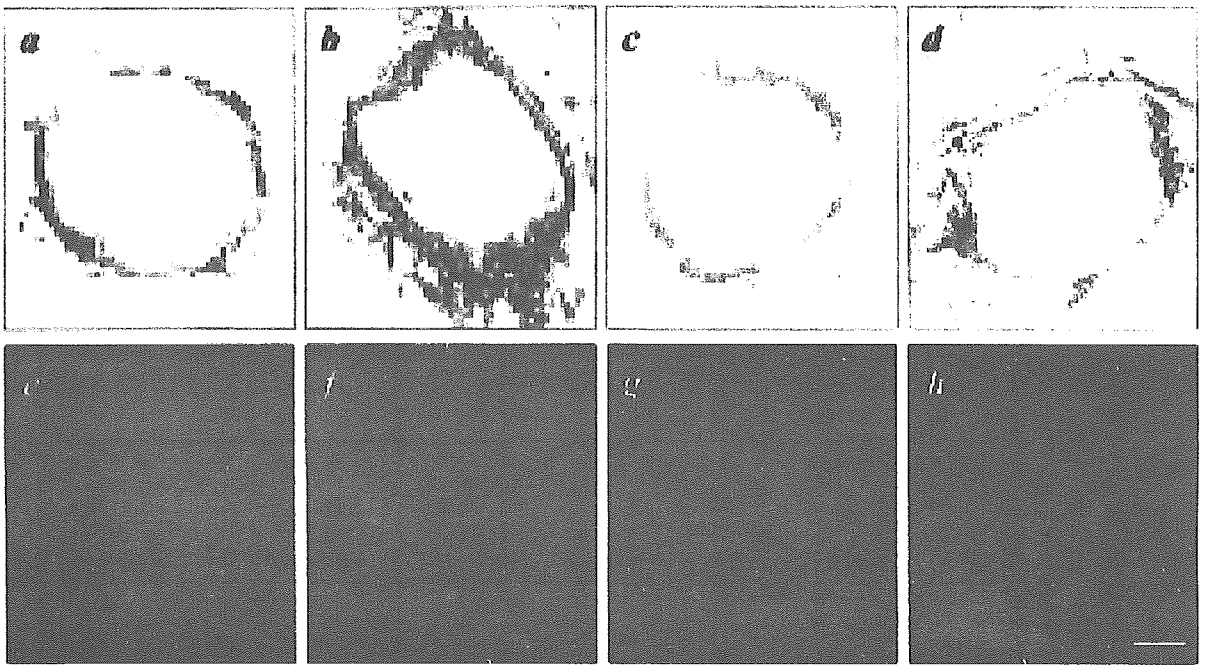

Fig. 2. *Representative micrograph of the effects of cilazapril and E4177 on vascular remodeling and perivascular collagen deposition in an intramyocardial artery. The sections were stained with Sirius red F3BA (a–d) and viewed through a polarized-light microscope (e–h). Arteries of WKY (a and e) and SHRSP treated with vehicle (b and f), cilazapril (c and g), and E4177 (d and h) are shown. Bar, 50 μm.*

Table 2. Wall-to-Lumen Ratio and Cross-Sectional Area of Intramyocardial Arteries, and Cardiac Collagen Area in 18-Week-Old Rats

Parameter	WKY	SHRSP	Cilazapril	E4177
Wall-to-lumen ratio	0.11±0.01	0.30±0.02*	0.22±0.02*,†	0.12±0.01†,§
Cross-sectional area (μm²/g)	9.4±1.9	53.0±4.8*	28.4±3.6*,†	13.1±1.6†,§
Perivascular collagen	0.7±0.1	2.0±0.2*	0.9±0.2†	0.8±0.2†
Interstitial collagen fraction (%)	1.1±0.2	2.5±0.3*	1.4±0.2†	0.8±0.1†

Values are the mean±SEM. WKY and SHRSP were treated with vehicle, cilazapril (10 mg/kg/day), and E4177 (30 mg/kg/day) for 6 weeks. *$p<0.01$, *vs.* the WKY groups, †$p<0.01$, ‡$p<0.05$ *vs.* the SHRSP group, §$p<0.01$ *vs.* the cilazapril group. WKY, Wistar-Kyoto rats; SHRSP, stroke-prone spontaneously hypertensive rats. Experiments, $n=8$.

wall-to-lumen ratio and cross-sectional area more than did cilazapril in SHRSP, and the ratio by E4177 reached the same level as was present in the WKY group. Both the perivascular and interstitial collagen deposition were significantly higher in the vehicle SHRSP group than in the WKY group. Both drugs significantly reduced the perivascular and interstitial collagen deposition compared with those in the vehicle SHRSP group, with no significant differences in values among the WKY group and the two drug-treated SHRSP groups.

Figure 3 shows that the vehicle SHRSP group had significantly higher cardiac levels of both 8-*iso*-$PGF_{2\alpha}$ and TBARS than did the WKY group. Both cilazapril and E4177 significantly inhibited the increase in both 8-*iso*-$PGF_{2\alpha}$ and TBARS in the SHRSP hearts, although the levels of 8-*iso*-$PGF_{2\alpha}$ in the cilazapril group were significantly higher than those in the WKY group. Furthermore, there was a significant difference between the ability of cilazapril and that of E4177 to prevent a rise in both 8-*iso*-$PGF_{2\alpha}$ and TBARS levels in the SHRSP hearts: E4177 almost entirely abolished the increases in both oxidative stress parameters, resulting in levels almost identical to those in the WKY group.

Figure 4A shows that $p22^{phox}$ expression was significantly upregulated in the vehicle SHRSP group compared with that in the WKY group. Both cilazapril and E4177 significantly downregulated $p22^{phox}$ expression compared with that in the vehicle SHRSP group. The E4177 group showed expression at almost the same level as that of the WKY group, whereas the level of $p22^{phox}$ expression in the cilazapril group was sig-

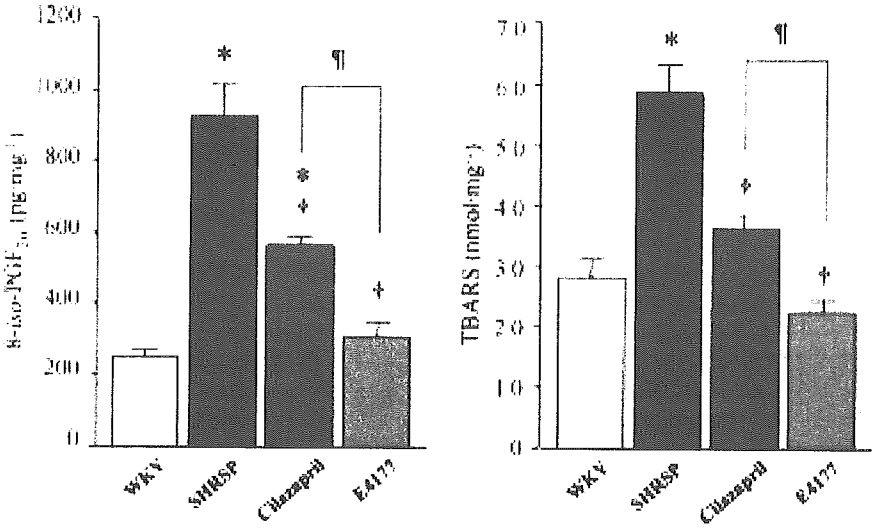

Fig. 3. *Levels of 8-iso-PGF2α and TBARS in rat hearts. Bars indicate SEM.* *$p < 0.01$ vs. *the WKY group,* †$p < 0.01$ vs. *the vehicle SHRSP group,* ¶$p < 0.05$ vs. *the cilazapril group. Experiments,* n = 8. *8-iso-PGF2α, 8-iso-prostaglandin F2α; TBARS, thiobarbituric acid reactive substances.*

nificantly higher than that of the WKY group. Inversely, Cu/ZnSOD expression was significantly downregulated in the vehicle SHRSP group compared with that in the WKY group. Compared to that in the vehicle SHRSP group, Cu/ZnSOD expression was significantly upregulated in both the cilazapril and E4177 groups, to levels almost equivalent to that in the WKY group. Furthermore, significant differences were seen between the cilazapril and E4177 groups in Cu/ZnSOD expression in SHRSP hearts. MnSOD expression in the heart was unaltered in each of the four groups.

Figure 4B shows the results of dual immunofluorescent staining of $p22^{phox}$, Cu/Zn-, or MnSOD, as well as α-SM actin and calponin 1 expression in the rat heart; it can be seen that $p22^{phox}$ was mainly localized not only in the media but also in the perivascular area of intramyocardial arteries in the vehicle SHRSP group, whereas $p22^{phox}$ was mainly localized only in the media of the intramyocardial arteries in the WKY group. Cardiac myocytes scarcely expressed $p22^{phox}$ in rat hearts. In contrast, Cu/ZnSOD and MnSOD were relatively and uniformly localized in the media of the intramyocardial arteries.

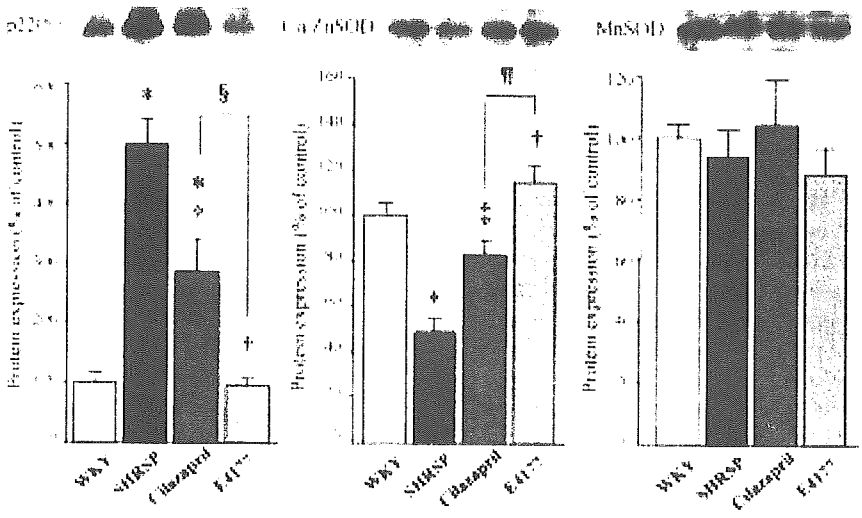

Fig. 4A. *Quantitative analysis of $p22^{phox}$, Cu/Zn-, and MnSOD expression in rat hearts. Bars indicate SEM.* *$p < 0.01$ vs. *the WKY group,* †$p < 0.01$, ‡$p < 0.05$ vs. *the vehicle SHRSP group,* §$p < 0.01$, ¶$p < 0.05$ vs. *the cilazapril group. Experiments,* n = 8.

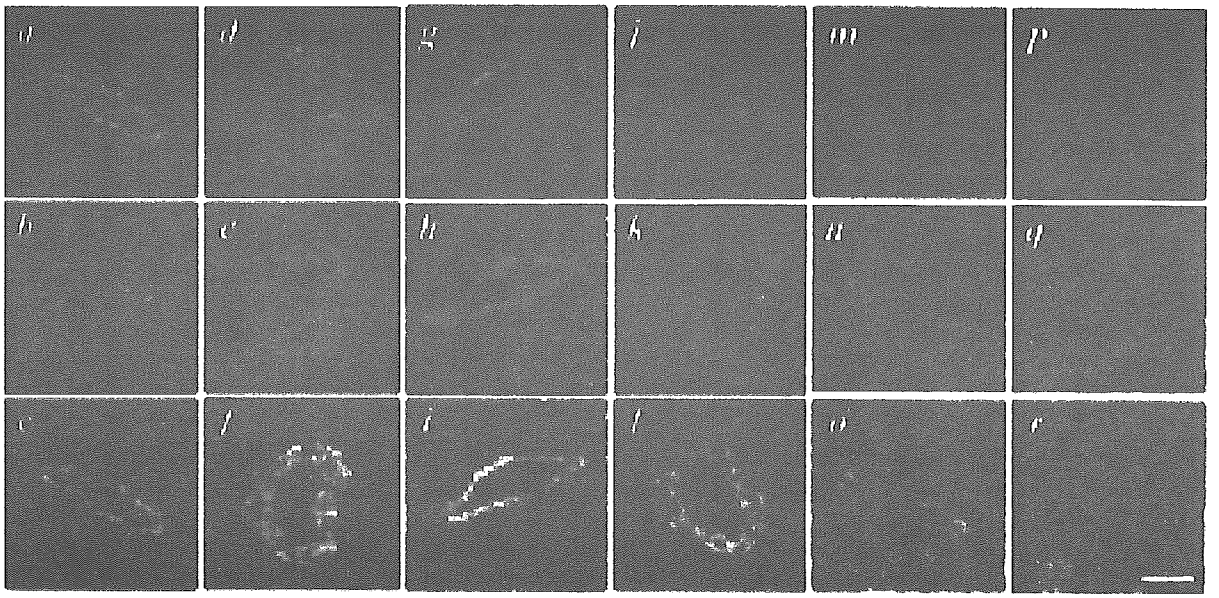

Fig. 4B. *Confocal microscopic analyses of the localization of $p22^{phox}$, Cu/Zn-, and MnSOD in an intramyocardial artery in rat hearts. Tissues were labeled with specific antibodies against α-SM actin (a, d, g, and j), calponin 1 (m and p), $p22^{phox}$ (b and e), Cu/ZnSOD (h and k), or MnSOD (n and q) in rat hearts. Arteries of WKY (a–c, g–i, and m–o) and SHRSP (d–f, j–l, and p–r) are shown. Merged images: α-SM actin with $p22^{phox}$ (c and f), Cu/ZnSOD (i and l) and calponin 1 with MnSOD (o and r). Bar, 50 μm.*

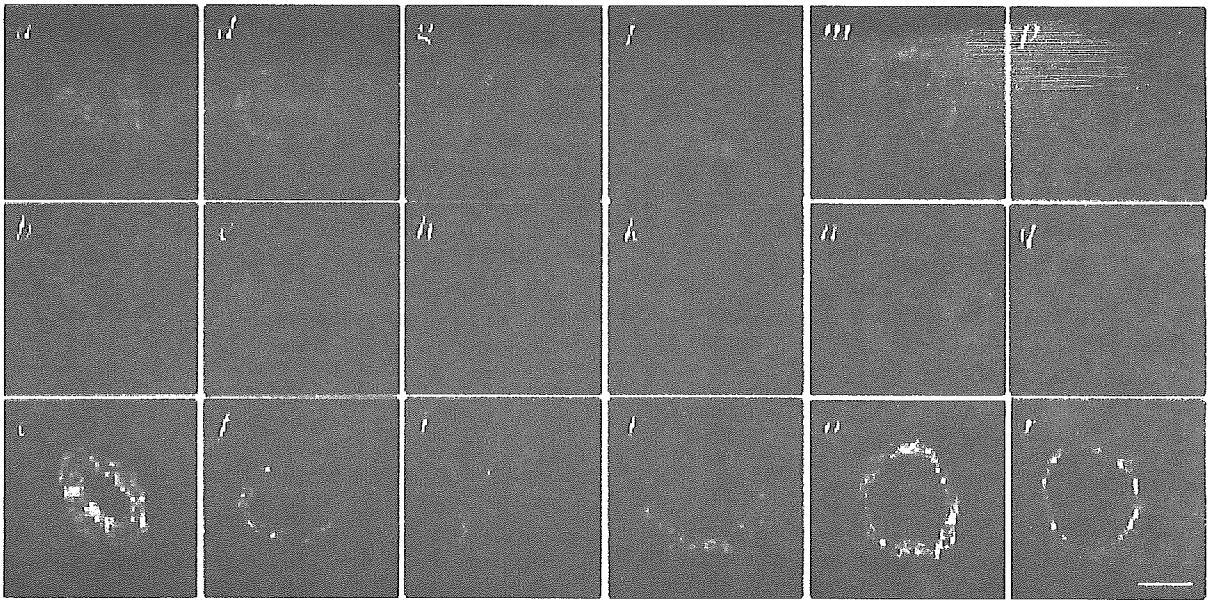

Fig. 4C. *Confocal microscopic analyses of the effects of cilazapril and E4177 on $p22^{phox}$ and Cu/ZnSOD in an intramyocardial artery in SHRSP hearts. Tissues were labeled with specific antibodies against α-SM actin (a, d, g, j, m, and p), $p22^{phox}$ (b, e, and h), and Cu/ZnSOD (k, n, and q) in SHRSP hearts. Arteries from animals in the vehicle SHRSP (a–c and j–l), cilazapril (d–f and m–o), and E4177 (g–i and p–r) groups are shown. Merged images: α-SM actin with $p22^{phox}$ (c, f, and i) and Cu/ZnSOD (l, o, and r). Bar, 50 μm.*

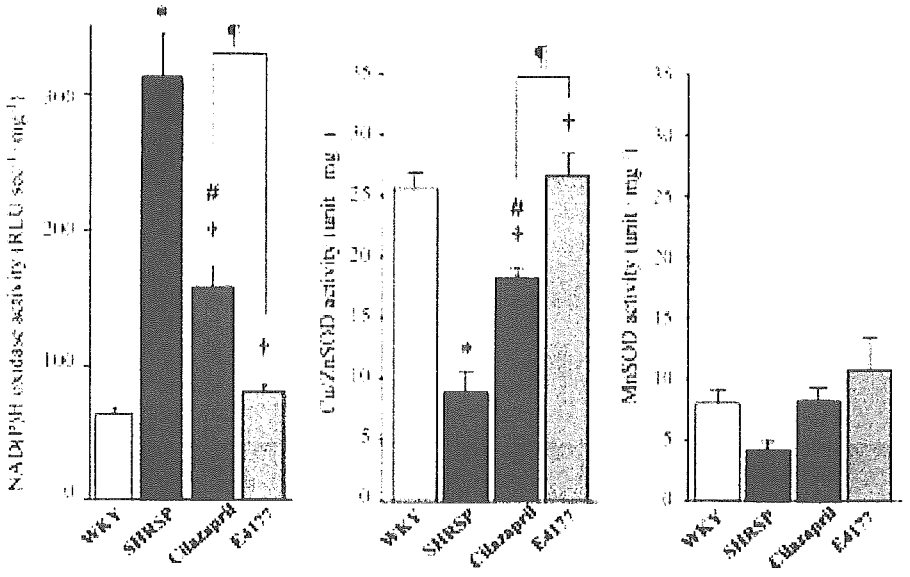

Fig. 5. *Quantitative analysis of NAD(P)H oxidase activity and Cu/Zn- and MnSOD activity in rat hearts. Bars indicate SEM.* *$p < 0.01$, #$p < 0.05$ vs. *the WKY group.* †$p < 0.01$ vs. *the vehicle SHRSP group.* ¶$p < 0.05$ vs. *the cilazapril group. Experiments,* $n = 4–5$.

but they were also found in cardiac myocytes in both the WKY and vehicle SHRSP groups. However, Cu/ZnSOD expression in cardiac myocytes was higher in the WKY group than in the vehicle SHRSP group.

Figure 4C shows the results of dual immunofluorescent staining of $p22^{phox}$ and Cu/ZnSOD, as well as α-SM actin expression in the SHRSP hearts. Both cilazapril and E4177 inhibited $p22^{phox}$ expression in the perivascular area and media of the intramyocardial arteries in the SHRSP heart, whereas Cu/ZnSOD expression was increased primarily in the perivascular area and media of the intramyocardial arteries as well as in cardiac myocytes of the SHRSP heart by the administration of cilazapril and E4177.

Figure 5 shows the results of the quantitative analysis of both NAD(P)H oxidase and SOD activities in rat hearts. NAD(P)H oxidase activity was significantly upregulated in the vehicle SHRSP group compared with the WKY group. Both cilazapril and E4177 significantly downregulated NAD(P)H oxidase activity compared to that in the vehicle SHRSP group. The E4177 group showed NAD(P)H oxidase activity at almost the same level as that of the WKY group, whereas the levels of NAD(P)H oxidase activity in the cilazapril group were significantly higher than those of the WKY group. In addition, there were significant differences in NAD(P)H oxidase activity in SHRSP hearts between the cilazapril and E4177 groups. Inversely, Cu/ZnSOD activity was significantly downregulated in the vehicle SHRSP group compared with that in the WKY group. Compared to that in the vehicle SHRSP group, Cu/ZnSOD activity in SHRSP hearts was significantly upregulated in both the cilazapril and E4177 groups. Cu/ZnSOD activity in the E4177 group improved to almost the same level as that of the WKY group, whereas Cu/ZnSOD activity in the cilazapril group was significantly lower than that of the WKY group. In addition, there were significant differences between the cilazapril and E4177 groups in Cu/ZnSOD activity in SHRSP hearts. MnSOD activity in the heart was not significantly different among the four groups.

The levels of eNOS expression in the rat heart were significantly downregulated in the vehicle SHRSP group compared with those in the WKY group (Fig. 6). Both cilazapril and E4177 caused significant upregulation of eNOS expression in SHRSP hearts, resulting in eNOS expression levels equivalent to those in the WKY hearts, while there were no differences in the degree of upregulation of eNOS expression in hearts between the two drug-treated SHRSP groups.

Discussion

The blood pressure-lowering actions of cilazapril and E4177 were accompanied by decreases in both oxidative stress and vascular hypertrophy, indicating that these processes are redox-sensitive in SHRSP (*6*), and equihypotensive effects of the two drugs were observed with the doses used in our study. We therefore conclude that the different mechanisms by which E4177 and cilazapril influence these processes could be related to the direct inhibiting action of ROS-generating enzyme systems and/or the upregulation of ROS-scavenging enzyme systems, as E4177 and cilazapril belong to two different classes of drugs. There are some differences in the mech-

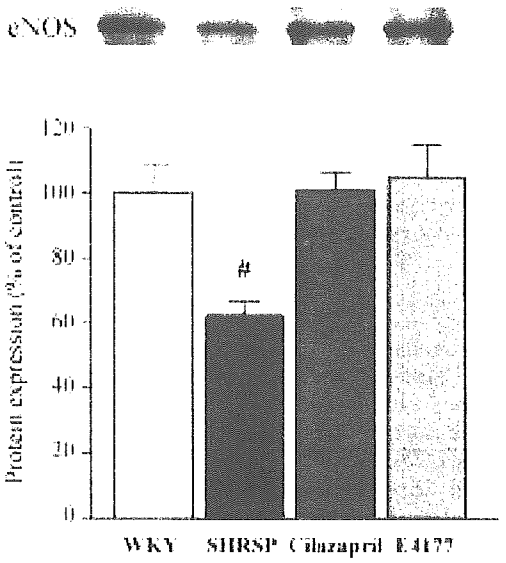

Fig. 6. *Quantitative analysis of eNOS expression in rat hearts. Bars indicate SEM.* $^{*}p < 0.05$ *vs. the WKY, cilazapril, and E4177 groups. Experiments,* $n = 8$.

anisms for blocking the renin-angiotensin system by the two drugs: cilazapril blocks Ang II formation, and hence less Ang II is available to stimulate both the AT1 and Ang II type 2 (AT2) receptors, whereas E4177 selectively blocks the AT1 receptor, causing the upregulation of Ang II formation and the stimulation of AT2 receptors. Activation of AT1 receptor by Ang II leads to phosphorylation of $p47^{phox}$ and subsequent translocation of $p47^{phox}$ to the membrane through the activation of phospholipase D, protein kinase C, and c-Src tyrosine kinase (*2*). This process promotes phosphorylated $p47^{phox}$ binding to the membrane component $p22^{phox}$ to activate NAD(P)H oxidase (*2*). In addition, it has been reported that the AT2 receptor function might be impaired in SHRSP, which could be responsible for the inappropriate progression of vascular remodeling in hypertension (*15, 16*), indicating that involvement of the AT2 receptor might be less than previously thought. These observations also indicate that the AT1 receptor, but not the AT2 receptor, plays a crucial role in vascular remodeling and NAD(P)H oxidase activity. Furthermore, aldosterone production in the vasculature may be involved in the results of our experiments. It has been shown that aldosterone is produced in the heart and blood vessels. The biological effects of aldosterone are mediated by the cardiac and vascular mineralocorticoid receptors, and the direct actions of Ang II, such as that of vascular remodeling *via* oxidative stress and inflammation of the vascular wall and heart, may be mediated in part by aldosterone (*17*). Furthermore, it has recently been suggested that Src activation by aldosterone is mediated through the mineralocorticoid receptor (*18*). Taken together with the previous report (*2*), these results suggest that NAD(P)H oxidase activity is regulated to some extent by aldosterone. Aldosterone selectivity in mineralocorticoid target tissues is primarily due to 11β-hydroxysteroid dehydrogenase, and diminished activity in resistance vessels of genetically hypertensive rats has also been shown (*19*). In the present study, we did not evaluate the effects of aldosterone on vascular remodeling in the SHRSP heart. However, recent studies have demonstrated that plasma aldosterone levels as well as plasma Ang II levels are not chronically suppressed by ACE inhibitors (*20*), whereas the AT1 receptor antagonist shows no evidence of aldosterone escape (*21*), suggesting that the effects of aldosterone escape in E4177 on vascular remodeling might be less than those in cilazapril.

Our immunofluorescence study has demonstrated that NAD(P)H oxidase assessed by the essential subunit of this enzyme, $p22^{phox}$, is primarily expressed in the media of intramyocardial arteries and the perivascular area in the heart, and that both cilazapril and E4177 downregulate the expression of $p22^{phox}$ in the perivascular area and the media of intramyocardial arteries in SHRSP hearts. Moreover, a significant difference in NAD(P)H oxidase activity as well as $p22^{phox}$ expression in SHRSP hearts was observed between the cilazapril and E4177 groups with the doses used in this experiment. Because NAD(P)H oxidase is the major source of superoxide anion in vascular cells (*1*), decreased activation of this enzyme by administration of the two drugs would result in reduced generation of superoxide anions in SHRSP hearts. In addition, both drugs were also found to reduce oxidative stress not only by decreasing NAD(P)H oxidase activity but also by selectively increasing Cu/ZnSOD expression and its activity, primarily in the perivascular area and media of the intramyocardial arteries, and also in cardiac myocytes of the SHRSP hearts. Furthermore, E4177 was found to reduce the concentrations of ROS to the same levels as those in the WKY group more efficiently than did cilazapril in SHRSP hearts, even though the E4177 group showed significantly higher SBP than the WKY group. These findings suggest that enhanced activation of Cu/ZnSOD in SHRSP hearts would lead to a further decrease in superoxide anion concentrations, and that E4177 may have additional benefits for the reduction of ROS in SHRSP hearts beyond the lowering of blood pressure. In earlier studies, antioxidants or chronic treatment with a SOD mimetic have been found to reduce oxidative stress, improve vascular function and structure, and prevent the progression of hypertension in SHRSP by altering the activation of vascular NAD(P)H oxidase and Cu/ZnSOD (*6, 22*). Furthermore, administration of Cu/ZnSOD within the vessel wall has been found to normalize the blood pressure of genetically hypertensive rats (*23*). It is also possible that both AT1 receptor antagonists and ACE inhibitors will improve endothelial function by accelerating the ROS-scavenging systems (*24*). Although we cannot elucidate which of the two ROS-related enzyme systems is more important, our results regarding the localization of Cu/ZnSOD and MnSOD in the rat heart are similar to those reported previously (*25*), and we observed, through comparisons between the two, that these

systems together could contribute to an overall reduction in the generation of ROS, improved oxidative status, and the inhibition of vascular remodeling of intramyocardial arteries in SHRSP. Our results are supported by Didion *et al.* (*26*), who clearly demonstrated that the selective loss of Cu/Zn-SOD results in increased superoxide and altered vascular responsiveness in both large arteries and microvessels in Cu/ZnSOD-deficient (Cu/ZnSOD$^{-/-}$) mice. The mechanisms by which E4177 and cilazapril influence Cu/ZnSOD are ill-defined, but the AT1 receptor might play an important role in the regulation of Cu/ZnSOD, based on the results observed in our study and those of an earlier report (*27*) which suggested that AT1 receptor function is involved in the regulation of Cu/ZnSOD. In addition, it has been reported that expression of the Cu/ZnSOD gene is induced by the inducible binding of peroxisome proliferators to peroxisome proliferator-activated receptors through the peroxisome proliferator-responsive element site, which is located between nt -797 and -786 of the 5′-flanking sequence of the rat Cu/ZnSOD gene (*28*), and that AT1 receptor antagonists induce peroxisome proliferators-activated receptor-γ activity (*29*). Taking the above together with our results, it is suggested that E4177 may upregulate Cu/ZnSOD activity through the activation of these processes in SHRSP hearts.

Increased vascular ROS production diminishes NO bioavailability and leads to endothelial dysfunction and vascular hypertrophy in hypertension (*30*). Although we did not measure NO activity in this study, it is possible that, even though cilazapril and E4177 had equipotent effects on the restoration of eNOS expression in SHRSP hearts, E4177 might provide additional benefits in terms of NO bioavailability. These processes could have been associated with attenuated vascular remodeling and reduced ROS in SHRSP *via* not only reductions in NAD(P)H oxidase levels but also upregulation of Cu/ZnSOD in our study.

In the present study, we did not examine the effects of E4177 and cilazapril on ROS-scavenging enzymes such as glutathione peroxidase and/or catalase in the rat heart (*31*). We cannot exclude the possibility that such ROS-scavenging enzymes as well as Cu/ZnSOD might affect ROS levels in the SHRSP heart. In addition, several reports have demonstrated that rat ecSOD is lacking in the vessel wall and is primarily present in plasma (*4*), and that ecSOD activity is quite low in the heart (*32*); as such, it is unlikely that ecSOD plays a critical role in the heart, although we cannot exclude the possibility that ecSOD in plasma could have influenced our results.

In summary, our study has demonstrated that E4177 and cilazapril might inhibit vascular remodeling in intramyocardial arteries of SHRSP *via* not only ROS-generating enzyme NAD(P)H oxidase but also through ROS-scavenging enzymes such as Cu/ZnSOD in the SHRSP heart. Although little is known about ROS-scavenging enzymes in hypertension *in vivo*, and further experiments will be necessary to examine the antioxidant properties of both agents, our findings provide a new view of hypertension and vascular remodeling, and present important information regarding the development of more effective therapies for hypertension.

Acknowledgements

We would like to thank Rie Ishihara and Kazuko Iwamoto for their excellent technical assistance and Dr. Tohru Fukai, Emory University, for his helpful discussions on ecSOD.

References

1. Griendling KK, Sorescu D, Lassegue B, Ushio-Fukai M: Modulation of protein kinase activity and gene expression by reactive oxygen species and their role in vascular physiology and pathophysiology. *Arterioscler Thromb Vasc Biol* 2000; **20**: 2175–2183.
2. Cai H, Griendling KK, Harrison DG: The vascular NAD(P)H oxidases as therapeutic targets in cardiovascular diseases. *Trends Pharmacol Sci* 2003; **24**: 471–478.
3. Dohi Y, Ohashi M, Sugiyama M, Takase H, Sato K, Ueda R: Candesartan reduces oxidative stress and inflammation in patients with essential hypertension. *Hypertens Res* 2003; **26**: 691–697.
4. Carlsson LM, Marklund SL, Edlund T: The rat extracellular superoxide dismutase dimer is converted to a tetramer by the exchange of a single amino acid. *Proc Natl Acad Sci USA* 1996; **93**: 5219–5222.
5. Fukai T, Folz RJ, Landmesser U, Harrison DG: Extracellular superoxide dismutase and cardiovascular disease. *Cardiovasc Res* 2002; **55**: 239–249.
6. Chen X, Touyz RM, Park JB, Schiffrin EL: Antioxidant effects of vitamins C and E are associated with altered activation of vascular NADPH oxidase and superoxide dismutase in stroke-prone SHR. *Hypertension* 2001; **38**: 606–611.
7. Matsumoto K, Morishita R, Moriguchi A, *et al*: Prevention of renal damage by angiotensin II blockade, accompanied by increased renal hepatocyte growth factor in experimental hypertensive rats. *Hypertension* 1999; **34**: 279–284.
8. Young AA, Legrice IJ, Young MA, Smaill BH: Extended confocal microscopy of myocardial laminae and collagen network. *J Microsc* 1998; **192**: 139–150.
9. Baba HA, Iwai T, Bauer M, Irlbeck M, Schmid KW, Zimmer HG: Differential effects of angiotensin II receptor blockade on pressure-induced left ventricular hypertrophy and fibrosis in rats. *J Mol Cell Cardiol* 1999; **31**: 445–455.
10. Fujii K, Umemoto S, Fujii A, Yonezawa T, Sakumura T, Matsuzaki M: Angiotensin II type 1 receptor antagonist downregulates nonmuscle myosin heavy chains in spontaneously hypertensive rat aorta. *Hypertension* 1999; **33**: 975–980.
11. Hermann M, Camici G, Fratton A, *et al*: Differential effects of selective cyclooxygenase-2 inhibitors on endothelial function in salt-induced hypertension. *Circulation* 2003; **108**: 2308–2311.
12. Kikugawa K, Kojima T, Yamaki S, Kosugi H: Interpretation of the thiobarbituric acid reactivity of rat liver and brain homogenates in the presence of ferric ion and ethylenediaminetetraacetic acid. *Anal Biochem* 1992; **202**: 249–255.
13. Nebot C, Moutet M, Huet P, Xu JZ, Yadan JC, Chaudiere J: Spectrophotometric assay of superoxide dismutase activity